

1 **Ocean Mesoscale and Frontal-scale Ocean-Atmosphere Interactions and**
2 **Influence on Large-scale Climate: A Review**

3
4
5 **US CLIVAR Mesoscale Air-Sea Interaction Working Group**

6 **Hyodae Seo*** (Woods Hole Oceanographic Institution, Woods Hole, MA, USA)

7 **Larry W. O'Neill** (Oregon State University, Corvallis, OR, USA)

8 **Mark A. Bourassa** (Florida State University, Tallahassee, FL, USA)

9 **Arnaud Czaja** (Imperial College London, London, United Kingdom)

10 **Kyla Drushka** (Applied Physics Laboratory, University of Washington, Seattle, WA, USA)

11 **James B. Edson** (Woods Hole Oceanographic Institution, Woods Hole, MA, USA)

12 **Baylor Fox-Kemper** (Brown University, Providence, RI, USA)

13 **Ivy Frenger** (GEOMAR Helmholtz Centre for Ocean Research Kiel, Germany)

14 **Sarah T. Gille** (Scripps Institution of Oceanography, University of California San Diego, La
15 Jolla, CA, USA)

16 **Benjamin P. Kirtman** (University of Miami, Miami, FL, USA)

17 **Shoshiro Minobe** (Hokkaido University, Sapporo, Japan)

18 **Angeline G. Pendergrass** (Cornell University, Ithaca, NY, USA)

19 **Lionel Renault** (LEGOS, University of Toulouse, Toulouse, France; Atmospheric and Oceanic
20 Sciences, University of California, Los Angeles, CA, USA)

21 **Malcolm J. Roberts** (Met Office Hadley Centre, Exeter, United Kingdom)

22 **Niklas Schneider** (University of Hawai'i at Manoa, Honolulu, HI, USA)

23 **R. Justin Small** (National Center for Atmospheric Research, Boulder, CO, USA)

24 **Ad Stoffelen** (Royal Netherlands Meteorological Institute, Utrecht, the Netherlands)

25 **Qing Wang** (Naval Postgraduate School, Monterey, CA, USA)

26
27
28
29
30
31
32
33
34
35
36
37
38
39
40
41
42
43
44
45
46

*Corresponding author: Hyodae Seo (hseo@whoi.edu)

47 **Abstract**

48 Two decades of high-resolution satellite observations and climate modeling studies have
49 indicated strong ocean-atmosphere coupled feedbacks mediated by small-scale oceanic
50 processes, including semi-permanent and meandering SST fronts, mesoscale eddies, and
51 filaments. The air-sea exchanges in latent heat, sensible heat, momentum, and carbon dioxide
52 associated with this so-called mesoscale air-sea interaction are found robust near the major
53 western boundary currents, Southern Ocean fronts, equatorial and coastal upwelling zones, but
54 they are also ubiquitous over the global oceans wherever ocean mesoscale processes are active.
55 Current theories, informed by rapidly advancing observational and modeling capabilities, have
56 established the importance of mesoscale air-sea interaction processes for understanding large-
57 scale ocean circulation, biogeochemistry, and weather and climate variability. However,
58 numerous challenges remain to diagnose, observe, and simulate mesoscale air-sea interaction
59 accurately to quantify its impacts on large-scale processes. This article provides a comprehensive
60 review of investigations of many key aspects pertinent to mesoscale air-sea interaction,
61 synthesizes current understanding with remaining gaps and uncertainties, and provides
62 recommendations on theoretical, observational, and modeling strategies for future air-sea
63 interaction research.

64
65

66 **Significance Statement**

67 Recent high-resolution satellite observations and climate models have characterized coupled
68 ocean-atmosphere interactions mediated by small-scale (mesoscale) ocean processes, including
69 ocean eddies and fronts. Ocean mesoscale-induced spatial temperature and current variability
70 modulate the air-sea exchanges in heat, momentum, and mass (e.g., gases such as carbon dioxide
71 and water vapor), altering coupled boundary layer processes. Studies suggest that skillful
72 simulations and predictions of ocean circulation, biogeochemistry, and weather and climate
73 events depend on accurate representation of the eddy-mediated air-sea interaction. However,
74 numerous challenges remain to diagnose, observe, and simulate mesoscale air-sea interaction
75 accurately to quantify its large-scale impacts. This article synthesizes the latest understanding of
76 mesoscale air-sea interaction, identifies remaining gaps and uncertainties, and provides
77 recommendations on strategies for future ocean-weather-climate research.

78 **1. Introduction**

79 Decades of observational and modeling analysis have broadly identified two fundamental
80 regimes of ocean-atmosphere coupling that are dependent on the spatial scale of ocean surface
81 variability. The first regime involves the ocean response to large-scale (>1000 km) atmospheric
82 internal variability, which drives a response in sea surface temperature (SST) through the
83 mediation of surface turbulent heat fluxes and upper-ocean turbulent mixing (e.g., Frankignoul et
84 al. 1985; Alexander and Scott 1997). The large-scale ocean response feeds back onto the
85 incipient atmospheric circulation anomaly to either reinforce or erode it (e.g., Bladé 1997). In
86 this framework, the ocean is viewed as relatively passive, mainly advecting anomalies, storing
87 heat, and serving as a source of noise forcing.

88
89 The second regime, the focus of this paper, involves an atmospheric response driven by
90 mesoscale eddy-induced spatial SST and current variability. Here, the term “mesoscale eddies
91 and fronts” broadly refers to all forms of oceanic processes with horizontal length-scales smaller
92 than the first regime of air-sea interaction (>1000 km) but larger than oceanic submesoscale (~10
93 km). These processes include coherent, swirling, and transient ocean circulations with length-
94 scales near the Rossby radius of deformation (Chelton et al. 2011), filamentary eddy structures
95 that are widely observed in coastal upwelling systems, and semi-permanent fronts and
96 undulations near the midlatitude western boundary currents (WBCs) and their extensions, and
97 SST fronts along the equatorial tongue in the Pacific and Atlantic oceans.

98
99 The SST signature from these ocean mesoscale processes modifies surface turbulent heat and
100 momentum fluxes, driving local responses in marine atmospheric boundary layer (MABL; e.g.,
101 Small et al. 2008), while MABL responses drive non-local responses in the path and activity of
102 storm tracks in the extratropics (e.g., Czaja et al. 2019) and deep moist convection in the tropics
103 (e.g., Li and Carbone 2012; Skillingstad et al. 2019; de Szoeke and Maloney 2020). The
104 atmospheric response to ocean mesoscales feeds back onto eddy activity and SST, and alters the
105 large-scale ocean circulation, further influencing these atmospheric processes (e.g., Nakamura et
106 al. 2008; Hogg et al. 2009; Frankignoul et al. 2011; Taguchi et al. 2012). The surface currents
107 from the ocean mesoscale eddies also affect the wind stress and heat fluxes as well as the wind
108 profiles in the MABL, which influence ocean circulation, including the stability and strength of

109 the WBCs (Renault et al. 2016b, 2019b) and the basin-scale coupled climate variability such as
110 ENSO (e.g., Luo et al. 2005). Ocean forcing of the atmosphere increases with time-scale and
111 decreases with increasing spatial scale (Bishop et al. 2017), suggesting the need to include
112 mesoscale eddies in coupled climate model simulations (e.g., Bryan et al. 2010; Kirtman et al.
113 2012; Roberts et al. 2016).

114

115 Aside from earlier limited observational studies showing the synoptic evidence of MABL
116 response to mesoscale SSTs (e.g., Sweet et al. 1981), the first global-scale surveys of the MABL
117 and surface wind responses were provided by Chelton et al. (2004) and Xie (2004), followed by
118 a comprehensive review paper by Small et al. (2008) and Kelly et al. (2010). The number of
119 publications that include aspects of mesoscale air-sea interaction has grown exponentially in the
120 last decade (See Robinson et al. 2018, 2020), which also emphasizes a strong cross-disciplinary
121 nature of the research subject, encompassing nearly all fields of atmospheric, oceanographic, and
122 climate sciences using theories, observations, and modeling (e.g., AMS Special Collection on
123 [Climate Implications of Frontal Scale Air-Sea Interaction](#), and the *J. Oceanography* Special
124 Collection on “Hot Spots” in the climate system, Nakamura et al. 2015). This review paper will
125 provide a synthesis of the latest advances in process-understanding from these investigations,
126 mainly focusing on work done in the last decade or so.

127

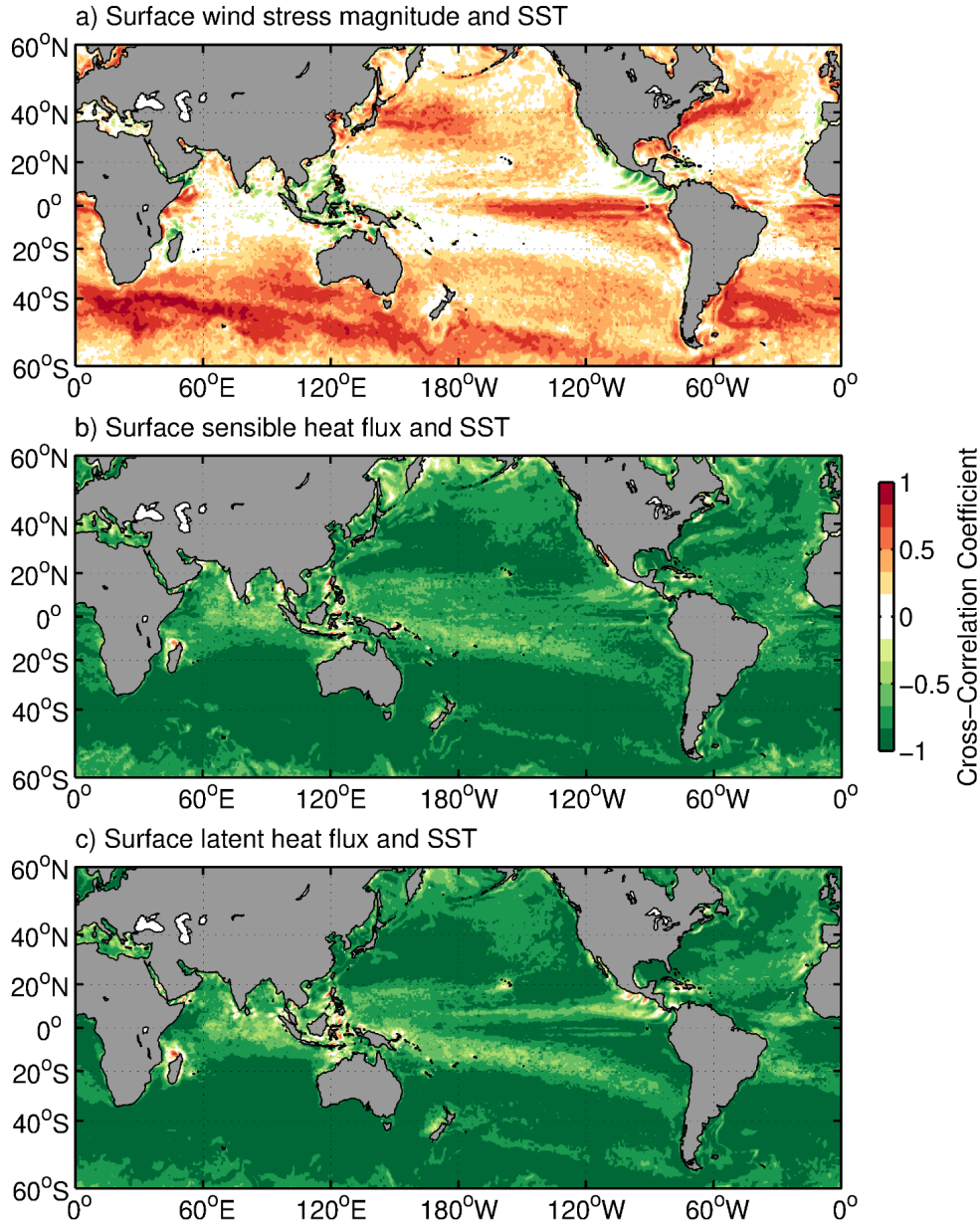
128 The paper is organized in the following way. The air-sea flux responses to mesoscale SST and
129 surface currents are discussed in Section 2, along with theories and analytical studies of MABL
130 dynamics describing the flux responses. Section 3 reviews the deep tropospheric responses,
131 emphasizing the modulation of local and downstream adjustments of extratropical weather
132 systems and their aspects related to climate change. Section 4 discusses thermal and mechanical
133 feedback effects on ocean circulation and biogeochemistry, and also explores theories and
134 parameterizations to account for eddy-atmosphere interaction. Section 5 discusses the emerging
135 observational platforms to enable accurate measurements of air-sea interaction at small spatial
136 scales. Section 6 provides a summary and discussion.

137

138 **2. Boundary layer and surface heat, momentum, and gas flux responses**

139 Surface fluxes communicate mass and energy between the ocean and atmosphere and are thus
140 key processes in Earth's climate system. The ocean is a major reservoir of heat and carbon in the
141 Earth system, and it is becoming increasingly clear that exchanges with the atmosphere occurring
142 on the oceanic mesoscale are significant in shaping Earth's climate. Recent assessments on
143 projected trends in surface air temperature (SAT) and SST have indicated a need to better
144 understand surface heat fluxes in part to reconcile conflicting lines of evidence on the projected
145 trends in SAT and SST (Box TS.1, IPCC 2021). The turbulent heat fluxes are composed of
146 sensible and latent heat fluxes, while the surface wind stress represents the turbulent momentum
147 flux between the atmosphere and ocean. This section discusses air-sea heat, momentum, and gas
148 flux responses to spatially heterogeneous fields of SST, surface currents, and sea state. We also
149 discuss the local MABL response to ocean-induced mesoscale forcing given its strong
150 relationship with the surface fluxes.

151
152 Surface flux response to spatially heterogeneous SST and currents generates responses initially
153 confined to the atmospheric and oceanic boundary layers, but feedbacks transfer the responses of
154 this coupling to the free atmosphere above (Section 3) and the ocean thermocline below (Section
155 4). Figure 1 shows the strong correlation between monthly mesoscale surface fluxes and ocean
156 mesoscale variability from the ERA5 reanalysis (Hersbach et al. 2020). When the local point-by-
157 point correlation correlations between the fluxes are strongly negative (with the sign convention
158 that the heat flux is positive downward), the SST variability can be viewed as the ocean forcing
159 the atmosphere. Similarly, when the correlation between turbulent heat flux and SST *tendency* is
160 negative, the atmosphere is viewed as driving ocean variability. Over mesoscale, the wind stress
161 and upward heat fluxes are enhanced over warm spatial SST anomalies (SSTA) and reduced over
162 cool SSTA. The correlations are much stronger for sensible and latent heat flux responses, while
163 the surface stress response on this spatial scale is much more apparent in oceanic frontal
164 boundary regions.



165
 166 **Figure 1:** Maps of the cross-correlation coefficients between ERA5 monthly spatially high-pass filtered SST
 167 and (a) wind stress magnitude, (b) surface sensible heat flux, and (c) surface latent heat flux. The spatial high-
 168 pass filter removed variability with spatial scales greater than 1000 km. The ERA5 reanalysis time period used
 169 here was 1991-2020. The standard sign convention for ERA5 surface fluxes is used: positive fluxes mean
 170 energy entering into the ocean.

171
 172 *a. Turbulent heat flux response*
 173 On smaller scales encompassed by the oceanic mesoscale and time-scales longer than synoptic
 174 time-scales, spatial variations in surface turbulent heat flux are driven primarily by spatial
 175 perturbations of SST, such that positive heat flux anomalies (i.e., ocean heat loss) occur over
 176 warm SST perturbations and negative heat flux anomalies (i.e., ocean heat gain) occur over cool

177 SST perturbations (Figure 1). Over these scales, the ocean forces a response of the atmosphere
178 driven by the surface heat exchange, which is fundamentally different from what occurs over
179 larger spatial scales. Near-surface air temperature and specific humidity adjust slowly to spatially
180 heterogeneous SST as air flows across SST fronts. Ocean mesoscale features and semi-
181 permanent WBCs often generate large air-sea temperature and humidity differences. The most
182 dramatic example was observed during the CLIMODE experiment near the Gulf Stream during
183 wintertime, when air-sea temperature differences exceeded 10°C over 200 km, yielding >1000
184 W/m^2 surface turbulent heat fluxes into the atmosphere (Marshall et al. 2009).

185

186 Past field experiments captured less extreme but nonetheless strong responses of turbulent heat
187 fluxes and MABL convective turbulence to mesoscale and frontal-scale SSTs. Examples can be
188 found from the Sargasso Sea during the FASINEX experiment (e.g., Friehe et al. 1991), Gulf
189 Stream (e.g., Plagge et al. 2016), Kuroshio (e.g., Tokinaga et al. 2009); Tropical Instability
190 Waves (Thum et al. 2002), Brazil-Malvinas Confluence system (e.g., Pezzi et al. 2005; Villas
191 Bôas et al. 2015; Souza et al. 2021), the Agulhas Current (e.g., Jury and Courtney 1991;
192 Messenger and Swart 2016), the western Arabian Sea (e.g., Vecchi et al. 2004).

193

194 The scale dependence has been quantified primarily from reanalysis-based surface flux and SST
195 datasets (e.g., Li et al. 2017; Sun and Wu 2021). Bishop et al. (2017), in particular, show that on
196 time-scales longer than one month, the turbulent heat fluxes on the oceanic mesoscale and frontal
197 scale are driven by SST variability associated with oceanic internal processes. On shorter time-
198 scales, the variability is driven more by synoptic-scale weather variability, particularly along the
199 storm tracks overlying the WBCs. Based on this simple diagnostic, Kirtman et al. (2012)
200 concluded that eddy-parameterized models grossly underestimate the ocean forcing of the
201 atmosphere in eddy-rich regions (i.e., WBCs and the Southern Ocean) and overestimate the
202 atmospheric forcing of the ocean throughout much of the mid-latitudes compared to the ocean
203 eddy-resolving simulations.

204

205 *b. Turbulent momentum flux and MABL wind responses*

206 The turbulent heat flux response to SST is a key process that drives the responses in turbulent
207 momentum flux to SST. The strong variability in ocean surface currents at mesoscales also affect

208 the wind stress through the relative motion of the surface winds and currents. The most
209 immediate local atmospheric response to SST and surface currents is initially confined to the
210 MABL. The wind and wind stress responses mainly result from a dynamical adjustment of the
211 MABL pressure and vertical turbulent stress profile distinct from simple adjustments of the
212 surface layer logarithmic wind profile (e.g., Small et al. 2008; O’Neill 2012; Renault et al.
213 2016a).

214

215 1) Mesoscale SST effects

216 Traditionally, local atmospheric responses to the mesoscale SST have been characterized by
217 empirical linear regressions between collocated mesoscale SSTs and surface winds and surface
218 wind stress, all spatially high-pass filtered to isolate the coupling on scales smaller than about
219 $O(1000\text{ km})$. Regression coefficients, called coupling coefficients, obtained from satellite-
220 observed wind speed and wind stress show ubiquitous increases of their magnitudes over warm
221 SSTs, increases of wind divergence and wind stress divergence co-located with the downwind
222 component of SST, and wind curl and wind stress curl that scale with crosswind components of
223 SST gradients (Chelton et al. 2001; O’Neill et al. 2003, 2012). The SST-induced curl and
224 divergence responses provide further constraints on spatial scales of the SST-induced MABL
225 response. These simple but powerful diagnostic metrics have helped to illuminate the simulated
226 air-sea interaction over a range of scales in numerical models (Bellucci et al. 2021), leading to
227 refinements in the SST resolution (Chelton 2005) and the PBL parameterizations in NWP
228 models (Song et al. 2017). However, in this approach, the wind responses to SST include
229 contributions from broad scales represented in high-pass filtered input fields. Alternative
230 diagnostic approaches exist, including cross-spectral analysis (e.g., Small et al. 2005b; O’Neill et
231 al. 2012; Laurindo et al. 2019; Samelson et al. 2020), cross-covariance and correlation functions
232 between SST (and its tendency), and wind and turbulent heat fluxes (e.g., Frankignoul and
233 Hasselmann 1977; Wu et al. 2006; Bishop et al. 2017; Small et al. 2019).

234

235 2) Mesoscale current effects

236 Regions of strong SST gradients are also regions of strong variability in ocean surface current.
237 The current feedback (CFB) mechanism directly modifies wind stress through the relative
238 motion of surface winds and currents, which in turn alters the low-level wind shear and wind: a

239 negative current anomaly induces a positive stress anomaly, which in turn causes a negative
240 wind anomaly (Renault et al. 2016a). At the mesoscale, CFB primarily impacts the surface wind
241 stress curl but not its divergence due to the quasi-geostrophic nature of ocean currents (Chelton
242 et al. 2004). The wind stress and wind responses to CFB can be also diagnosed using empirical
243 relationships based on satellite and numerical simulations. Renault et al. (2016a; 2019a) defined
244 two coupling coefficients related to CFB: s_w is the slope of the regression between mesoscale
245 surface currents and 10 m wind and s_τ is the linear regression coefficient linking mesoscale
246 surface current and surface stress. The coefficient s_τ can be interpreted as a measure of the CFB
247 efficiency: the more negative s_τ , the more efficient an eddy killing. The effect on the ocean is
248 discussed in detail in Section 4.

249
250 The SST and current-induced stress responses are challenging to separate since mesoscale SST
251 and current variations tend to co-vary strongly near ocean fronts and eddies. Nonetheless,
252 estimates of the contributions of the current-induced wind stress response via the linear coupling
253 coefficients indicate that the current-induced stress anomalies exceed the SST-induced response
254 over strong WBCs and within isolated ocean eddies (e.g., Gaube et al. 2015; Renault et al.
255 2019a). The current-induced stress response exists in scatterometer and direct air-sea flux
256 observations and coupled ocean-atmosphere simulations but is not directly apparent in
257 atmosphere-only simulations and reanalyses, such as the ERA5 wind stress anomalies used in
258 Figure 1. Including both current and SST-induced stress anomalies has a particularly strong
259 impact on the mesoscale wind stress curl field.

260 261 *c. Analytic framework for SST-induced boundary layer response*

262 The MABL response to ocean mesoscale current must incorporate coupling between the MABL
263 thermodynamics and dynamics to adequately represent the influence of SST and surface current
264 on the surface wind stress and sensible and latent heat fluxes. An analytical framework for SST
265 impacts was recently proposed, which incorporates MABL heat and momentum budgets that
266 capture the first-order response of the MABL to SST forcing (Schneider and Qiu 2015;
267 Schneider 2020) and includes representation of the processes shown in the literature to be of
268 primary importance. This framework considers an MABL capped by an inversion (Battisti et al.
269 1999). Within this layer, air temperature is assumed well mixed and vertically constant and

270 subject to horizontal advection and air-sea heat exchanges. The system is driven by winds with
 271 horizontal scales far larger than the ocean mesoscale that satisfy a drag law at the sea surface and
 272 experiences zero vertical momentum flux at the inversion. The large-scale winds \vec{U} form a
 273 modified Ekman spiral (Holton 1965a,b), which is considered horizontally homogeneous on
 274 scales commensurate with the ocean mesoscale.

275

276 SST T enters the heat budget of the layer via the air-sea heat exchanges due to the air-sea
 277 temperature difference with rate γ . Air temperature θ results to first order from a steady balance
 278 of surface sensible heat fluxes with advection by large-scale winds (e.g., Small et al. 2005a),

279

$$\vec{U} \cdot \nabla \theta = \gamma(T - \theta).$$

280

281

282 The MABL air temperatures θ adjust to T over a length-scale of U/γ , forming a wake of
 283 elevated values of the air-sea temperature differences in the lee of spatial SST variations.

284 Thermal adjustment rates of the boundary layer γ correspond to adjustment times of the order of
 285 a few hours to half a day (Schubert et al. 1979), yielding length scales of $O(100 \text{ km})$. The
 286 momentum equations govern the wind response to the ocean mesoscale SST-induced
 287 acceleration \vec{F} ,

$$\vec{U} \cdot \nabla \vec{u} + \frac{w^*}{H} \partial_s \vec{U} + f \hat{e}_3 \times \vec{u} - \frac{1}{H^2} \partial_s A \partial_s \vec{u} + g' \nabla h = \vec{F},$$

288

289 which include on the lhs horizontal advection by large-scale winds \vec{U} of SST induced winds \vec{u}
 290 and vertical advection w^* of the large-scale shear, the Coriolis acceleration with Coriolis
 291 frequency f , the divergence of vertical fluxes of horizontal momentum due to large-scale mixing
 292 with eddy coefficient A , and hydrostatic pressure gradient forces, including the so-called back
 293 pressure effect (e.g., Hashizume et al. 2002) due to ocean mesoscale-induced changes of
 294 inversion height h . Together with the continuity equation and boundary conditions of a drag law
 295 at the sea surface, and a material inversion with no flux of momentum, these equations provide a
 296 complete analytical solution for the wind response to ocean mesoscale SSTs.

297

298 Changes of θ impact accelerations \vec{F} to the horizontal momentum on the rhs through the
 299 hydrostatic pressure term, which couples the MABL thermodynamics with the dynamics:

300

$$\vec{F} = \frac{gH}{\Theta_0}(1-s)\nabla\Theta + \frac{1}{H^2}\partial_s(\dot{A}\partial_s\vec{U}) \quad (1)$$

301

302 through the modulation of the hydrostatic pressure gradients (the first term on the right), and the
303 sensitivity of the vertical mixing to the fluxes at the air-sea interface (the second term on the
304 right). The sigma vertical coordinate s measures the height relative to the mean inversion height
305 H , Θ_0 is a reference temperature, g the earth's gravitational acceleration, and \dot{A} is the sensitivity
306 of vertical mixing A to SST.

307

308 The vertical mixing effect, the second term on the right on Eq. (1), is a linearization of the
309 'nonlinear' term envisioned by Wallace et al. (1989) and Hayes et al. (1989) that captures the
310 modulations of the vertical mixing acting on the large-scale wind profile. The dynamics,
311 amplitude, and vertical structure of \dot{A} determine the character of mixing sensitivity. Mixing can
312 intensify and change its vertical scale. The dependence of vertical mixing on the non-equilibrium
313 air-sea temperature difference is but one possibility. Alternatively, SST induces convective
314 adjustment of the lapse rate and permanently deepens the boundary layer over warmer waters
315 (Samelson et al. 2006). These diagnostic formulations for \dot{A} are endpoints of the non-equilibrium
316 evolution of vertical mixing simulated by LES (e.g., de Szoeke and Bretherton 2004;
317 Skyllingstad et al. 2007; Sullivan et al. 2020), which allow for changes of the vertical mixing
318 that lag modulations of boundary layer stability (Wenegrat and Arthur 2018). As such, the
319 coupling between surface winds and SST is sensitive to the MABL turbulence closure schemes
320 (e.g., Song et al. 2009, 2017; Perlin et al. 2014; Samelson et al. 2020).

321

322 Advection by large-scale winds allows for disequilibrium in air-sea temperature and shifts
323 responses of winds or stress as a function of the SST spatial scales and the large-scale wind
324 direction and speed (e.g., Small et al. 2005a, 2008). Spectral transfer functions, or their
325 corresponding physical-space impulse response functions, capture these non-local relationships,
326 and generalize the widely used coupling coefficients to include spatial lags. Estimates from
327 satellite observed winds and SST of spectral transfer functions suggest scale-dependent, lagged
328 dynamics as a function of the Rossby number determined by large-scale winds, the wavenumbers
329 of ocean mesoscale SST and the Coriolis frequency f , or thermal or frictional adjustment rates γ

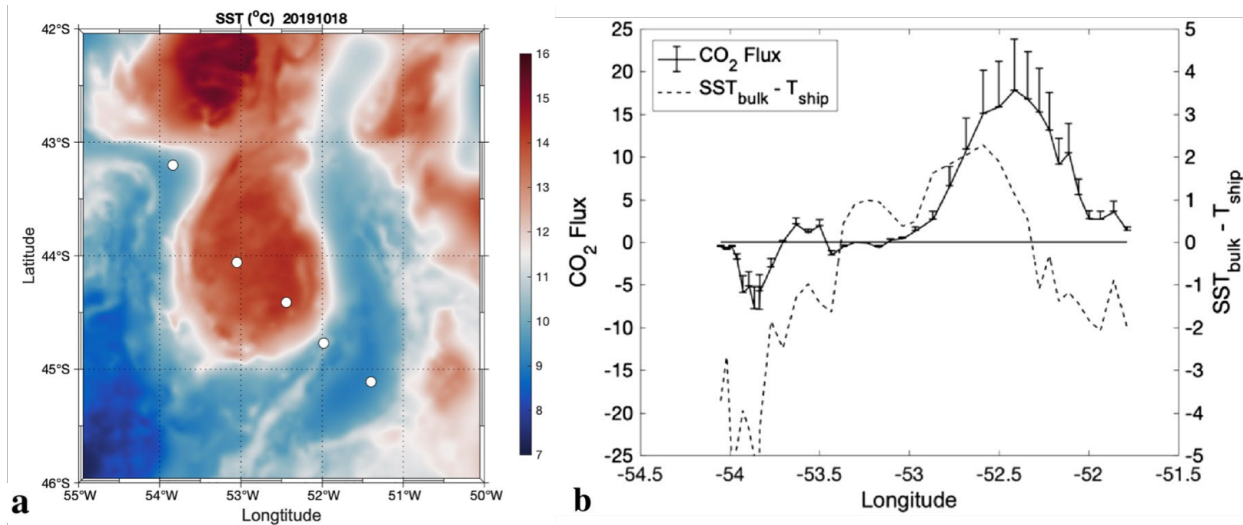
330 or A/H^2 (Schneider 2020; Masunaga and Schneider 2021). For small Rossby numbers the
331 pressure effect dominates, large Rossby numbers favor the vertical mixing effect, and order one
332 Rossby numbers combine both with rotational effects, consistent with modeling studies of
333 boundary layer responses to prototype SST fronts (Spall 2007; Kilpatrick et al. 2014, 2016) and
334 ocean eddy fields (Foussard et al. 2019a) in the presence of large-scale winds.

335
336 The analytical model described above considers a dry MABL without incorporating MABL
337 moisture or latent heat fluxes. The contribution of moisture to buoyancy fluxes, latent
338 heating/cooling, and overall MABL structure has not been investigated in as much detail within
339 the context of the mesoscale MABL response. However, it is anticipated to have a non-negligible
340 impact on the MABL dynamical response to mesoscale SSTA (Skyltingstad and Edson 2009).
341 For instance, during CLIMODE, the buoyancy heat flux was approximately 20% larger than the
342 sensible heat flux due to moisture and the average magnitude of the latent heat flux was ~ 2.5
343 times greater than the sensible heat flux (Marshall et al. 2009). In the tropics, the ratio of latent to
344 sensible heat flux is even larger (e.g., de Szoeke et al. 2015), so the moisture contribution is often
345 an order of magnitude larger than the sensible heat contribution. The impact of moist convection
346 during a cold air outbreak over the Gulf Stream was investigated with an LES (Skyltingstad and
347 Edson 2009), showing that the latent and sensible heat fluxes are enhanced over a simulated SST
348 front resulting in stronger turbulent mixing and precipitation compared to a constant SST
349 simulation. The simulation across the SST front shows that relatively low humidity values near
350 the surface are maintained by the continual expansion of the boundary layer in the entrainment
351 layer, which mixes dry air from aloft into the MABL. This maintains the large air-sea specific
352 humidity and temperature differences necessary for strong latent and sensible heat fluxes in the
353 surface layer. Additional simulations and measurements are necessary to investigate the role of
354 moisture in response to mesoscale SST. For example, the analytical model could provide insight
355 by using the virtual temperature at both the sea surface and aloft.

356
357 *d. Modulation of air-sea fluxes of tracers*

358 Air-sea gas fluxes of tracers depend on the air-sea disequilibrium and processes driving
359 exchange, such as winds and breaking waves. From the ocean perspective, the disequilibrium can
360 be understood as the difference of the concentrations of a gas in the seawater, C , relative to the

361 concentration the gas would have at equilibrium with the atmosphere, C_{eq} , which, in turn, is
 362 determined by the solubility of the gas in seawater. The air-sea flux F then is estimated as $F =$
 363 $k(C - C_{eq})$, where k is the gas transfer velocity (e.g., Woolf 1993; McGillis et al. 2001;
 364 Wanninkhof et al. 2009; Dong et al. 2021). Impacts of ocean mesoscale features on the net F may
 365 be introduced via k or C_{eq} , each of which varies nonlinearly with wind speed and depends on sea
 366 state. The mesoscale may also affect C by impacting biological sources and sinks of tracers
 367 (Section 4d). Indeed, studies find local modulations of air-sea CO_2 fluxes due to effects of
 368 mesoscale eddies on solubility, productivity, or winds (Jones et al. 2015; Song et al. 2015, 2016;
 369 Olivier et al. 2021). One such study in the Southwest Atlantic Ocean detected clear spatial
 370 covariations of CO_2 flux with the MABL stability over a warm-core eddy (Figure 2, Pezzi et al.
 371 2021). Yet, on the basin-to-global scales, positive and negative mesoscale anomalies of CO_2
 372 fluxes appear to largely cancel (Wanninkhof et al. 2011; Song et al. 2015). A clear separation
 373 and quantification of the individual and rectified effects of mesoscale phenomena on k , C , and
 374 C_{eq} from observations and models remain challenging, given the difficulty to capture transient
 375 mesoscale variations in the ocean and atmosphere, including the concentration of tracers such as
 376 carbon.
 377



378 **Figure 2:** (a) Observed SST ($^{\circ}\text{C}$) in the Southwestern Atlantic Ocean on 18 October 2019. The white circles
 379 denote the Po/V *Almirante Maximiano* trajectory. (b) In situ CO_2 fluxes ($\mu\text{mol m}^{-2}\text{s}^{-1}$) measured by Eddy
 380 Covariance method (solid) and atmospheric stability parameter $\text{SST} - T_{\text{air}}$ ($^{\circ}\text{C}$) (dotted). The error bars denote
 381 the standard error representing a 95% confidence interval. Figures adapted from Pezzi et al. (2021).
 382

383 **3. Free-tropospheric, extratropical atmospheric circulation responses**

384 This section investigates local and non-local atmospheric circulation responses to extratropical
385 SSTA including WBC regions. We start with a summary of existing studies on the role of
386 extratropical SSTA in quasi-equilibrium atmospheric circulation and storm tracks. We then
387 discuss the ongoing debates about the observed near-surface wind convergence and precipitation
388 in WBC regions diagnosed either as a response to SST variations or extratropical storms. Finally,
389 we will consider whether these processes may be important to future climate, focusing on the
390 difference between projections at high and low resolution in the oceans.

391

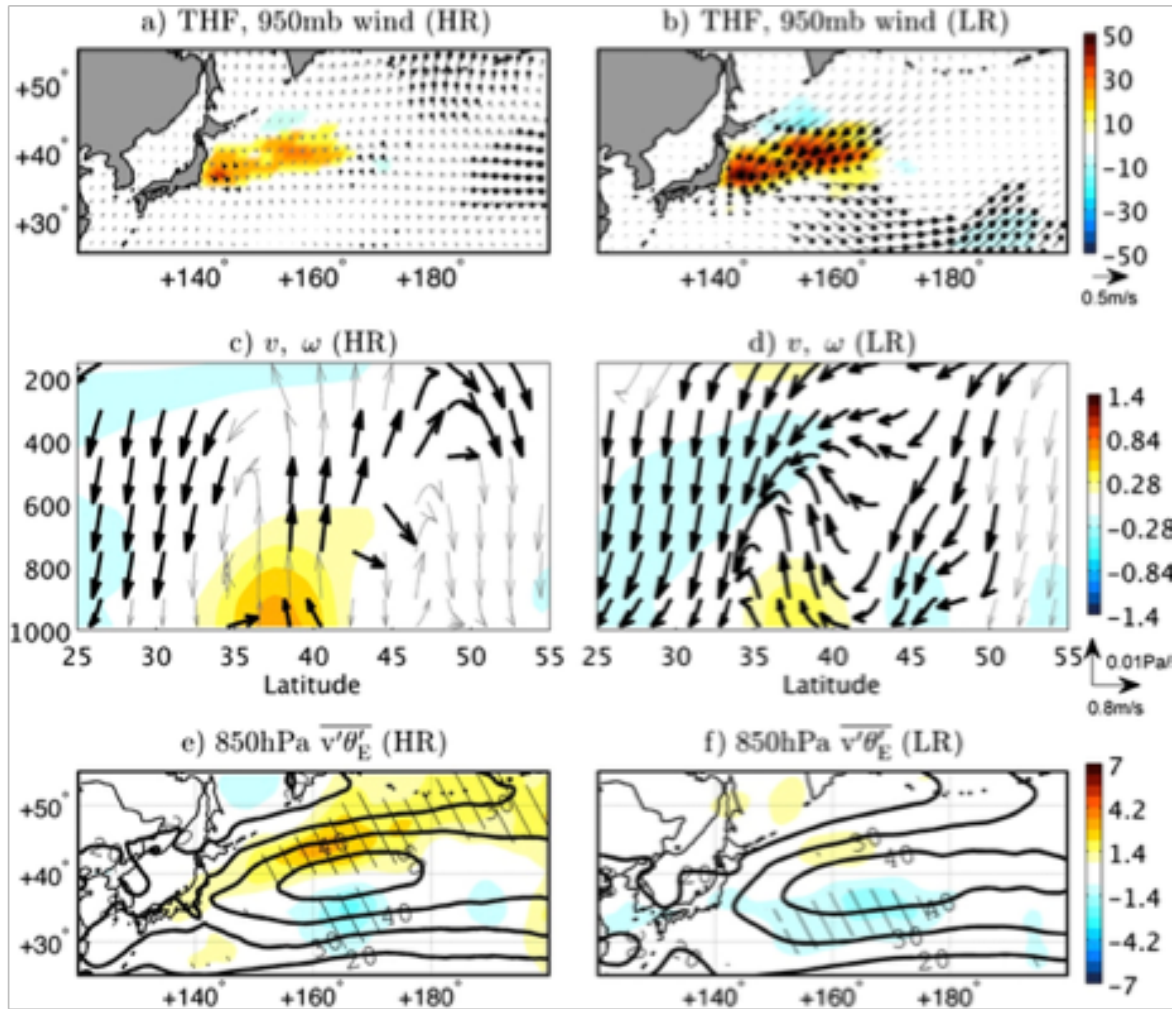
392 *a. Time-mean general circulation responses*

393 The question of how the extratropical atmosphere responds to variability in ocean fronts and/or
394 extratropical SSTA has been addressed over many decades. Early studies considered the linear
395 response (Hoskins and Karoly 1981; Frankignoul 1985), which predicted a shallow heating
396 response characterized by a downstream trough with a baroclinic structure. This was argued
397 against by Palmer and Sun (1985), who found a downstream ridge, with advection of
398 temperature anomalies by mean flow acting against anomalous advection of mean temperature
399 gradients. Later, Peng et al. (1997) showed that the transient eddy response was important in
400 forming an equivalent barotropic high. More recent observational analyses find a weak low-
401 pressure response east of warm SSTA near the Gulf Stream (Wills et al. 2016) and Kuroshio
402 (Frankignoul et al. 2011; Wills and Thompson 2018). Deser et al. (2007) demonstrated that the
403 initial linear, baroclinic response is quickly (within 2 weeks) replaced with the equilibrium
404 barotropic response with a much broader spatial extent and magnitude (Ferreira and Frankignoul
405 2005, 2008; Seo et al. 2014). The adjustment time is shorter near WBC regions (Smirnov et al.
406 2015). This literature is well summarized in existing review papers (Kushnir et al. 2002; Small et
407 al. 2008; Kwon et al. 2010; Czaja et al. 2019).

408

409 Recent studies also indicated a strong sensitivity on spatial resolution of the atmospheric
410 dynamics governing the large-scale circulation response. Figure 3 from Smirnov et al. (2015)
411 shows that a low-resolution (1°) model induces a weak response resulting from shallow
412 anomalous heating balanced by equatorward cold air advection, consistent with the results from
413 linear steady dynamics. This is in contrast to the higher resolution ($1/4^\circ$) model showing that the

414 anomalous diabatic heating is balanced by a deep vertical motion mediated by the transient
 415 eddies (Hand et al. 2014; Wills et al. 2016; Lee et al. 2018). The anomalous diabatic heating and
 416 the induced vertical motions maintain the climatological circulation pattern over the WBCs.
 417



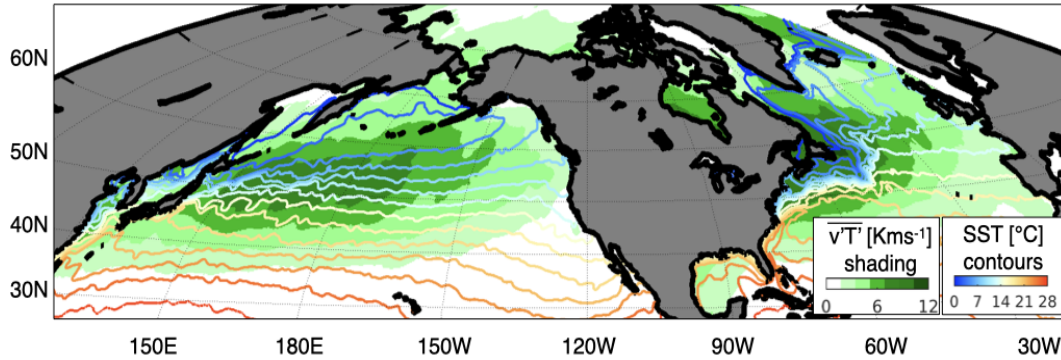
418
 419 **Figure 3:** The mean DJF atmospheric response to a shift in the Oyashio Extension SST front in (left) high ($\frac{1}{4}^\circ$)
 420 and (right) low (1°) resolution AGCM simulations. (a-b) Turbulent heat flux (colors; Wm^{-2}) and 950-hPa wind
 421 (vectors; ms^{-1}). (c-d) Zonally averaged ($145\text{--}165^\circ\text{E}$) across-front circulation and equivalent potential
 422 temperature (θ_E , colors). (e-f) The 850-hPa poleward energy flux ($\overline{v'\theta'_E}$, colors Kms^{-1}). The black contours
 423 indicate climatology. Significant response at 95% confidence level is indicated as thick vectors and stippling.
 424 From Smirnov et al. (2015).
 425

426 *b. Synoptic storms and storm track responses*

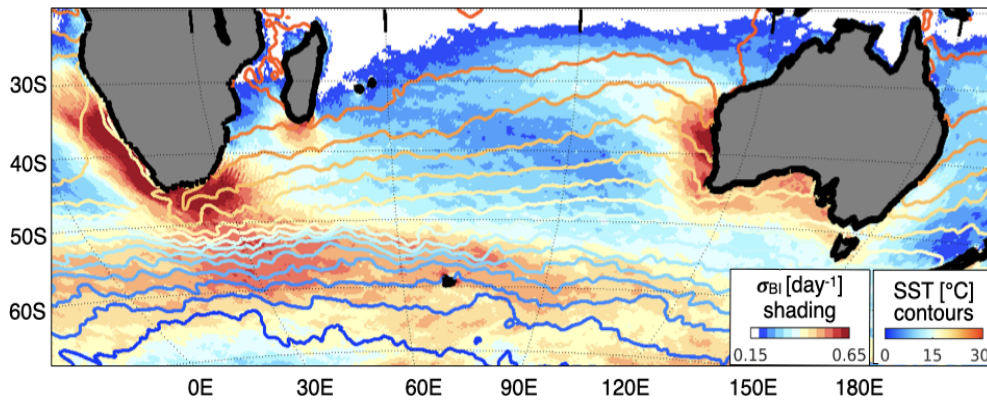
427 Midlatitude storm tracks can be largely defined in two ways (Chang et al. 2002; Hoskins and
 428 Hodges 2002): either using distributions of the tracks and intensity of synoptic cyclones (the

429 Lagrangian view) or as regions of strong variability or co-variability of winds, geopotential
 430 height, temperature, and humidity (the Eulerian perspective). Storm tracks typically occur in the
 431 30-50° latitude band coincident with the climatological SST fronts (Figure 4) and are associated
 432 with strong and frequent precipitation, particularly atmospheric fronts.
 433

(a) Climatological storm track over Kuroshio and Gulf Stream



(b) Climatological “baroclinicity” over Agulhas and ACC



434
 435 **Figure 4:** This figure illustrates the climatological relationship of the extratropical storm tracks with the SST
 436 fields in (a) Kuroshio-Oyashio Extension and Gulf Stream in the Northern Hemisphere, and (b) Agulhas
 437 Current and the Antarctic Circumpolar Current systems in the south Indian Ocean. The atmospheric storm
 438 track is estimated in (a) as the time-mean meridional heat transport by transient eddies, $\overline{v'T'}$, at 850 hPa (low
 439 troposphere), where primes denote the 2-8-day bandpass filtered fields and the over-bar indicates the time-
 440 mean, and in (b) as the maximum Eady growth rate, defined as the most unstable baroclinic mode whose
 441 growth rate is scaled as the magnitude of the baroclinicity vector, $|\sigma_{BI}| = 0.31 \left(\frac{g}{N\theta} \right) \left| -\frac{\partial\theta}{\partial y}, \frac{\partial\theta}{\partial x} \right|$, at 850 hPa,
 442 where g is the gravitational acceleration, N is the buoyancy, and θ is the potential temperature. These storm
 443 track quantities are derived from ERA5. The SST climatology is obtained from the NOAA daily Optimum
 444 Interpolation dataset. The climatologies are calculated from 2010 to 2015.
 445

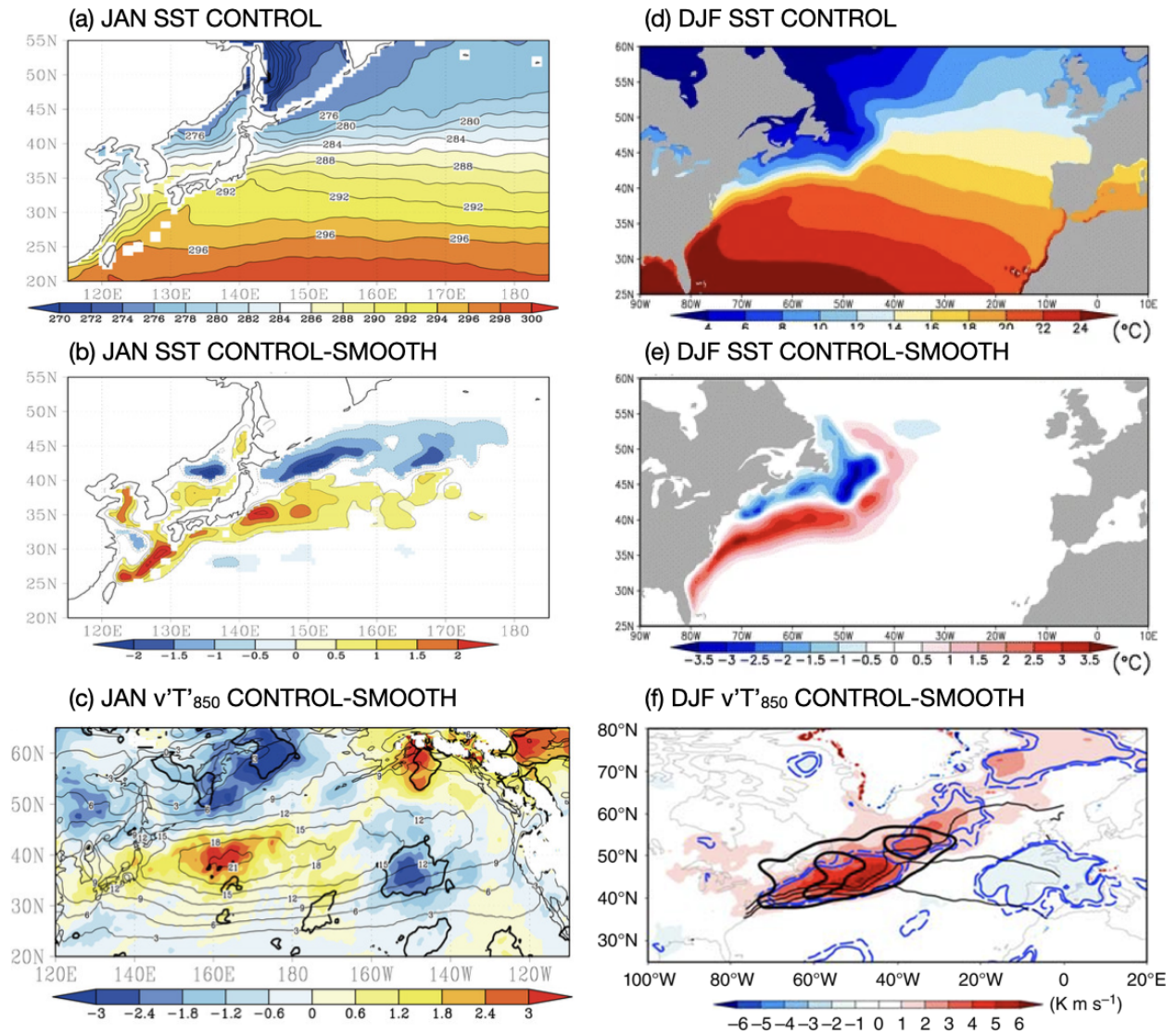
446 One possible mechanism of midlatitude oceanic influence on the storm track was suggested by
 447 Hoskins and Valdes (1990), who found that enhanced diabatic heating by surface fluxes over
 448 WBCs supports atmospheric baroclinicity, a vital element in setting the location of the storm

449 track (Hawcroft et al. 2012; Kaspi and Schneider 2013). Nakamura and Shimpo (2004) and
450 Nakamura et al. (2004) further argued that low-level air temperature gradients are directly
451 influenced by SST gradients via cross-frontal gradients in sensible heat flux (See also Nakayama
452 et al. 2021). The baroclinicity is measured as the maximum Eady growth rate (Charney 1947;
453 Eady 1949; Lindzen and Farrell 1980), such that stronger low-tropospheric baroclinicity is
454 associated with weaker static stability and a stronger meridional air temperature gradient. Both
455 conditions can be observed over WBCs. Hence, the anchoring effect by cross-frontal differential
456 heat supply from the ocean is consistent with the formation of a storm track (Nonaka et al. 2009;
457 Hotta and Nakamura 2011), while diabatic heating over the warm portion of the WBC SST
458 fronts to the warm and cold sectors of the cyclones supports the growth of transient baroclinic
459 waves (e.g., Booth et al. 2012; Willison et al. 2013; Hirata and Nonaka 2021).

460

461 A common method to diagnose the SST forcing mechanism is to run a pair of AGCM
462 simulations, one using observed SSTs (CONTROL), and another using a spatially-smoothed SST
463 field with weaker gradients (SMOOTH), which also alters absolute SST. Alternatively, AGCMs
464 are forced by shifting the latitude of the SST fronts or filtering mesoscale eddy SSTs. Such
465 AGCM simulations indicate a strengthening of the storm track near the Kuroshio-Oyashio
466 Extension (KOE) (Kuwano-Yoshida and Minobe 2017) and the Gulf Stream (O'Reilly et al.
467 2017) in CONTROL near the climatological maximum cyclogenesis (Figure 5). Altered storm
468 activity over the WBC regions influences the intensity of the coastal storms, and thereby inland
469 weather near the KOE (Nakamura et al. 2012; Hayasaki et al. 2013; Sugimoto et al. 2021), Gulf
470 Stream (Infanti and Kirtman 2019; Hirata et al. 2019; Liu et al. 2020), and the Agulhas Current
471 (Singleton and Reason 2006; Nkwinkwa Njouodo et al. 2018).

472



473
 474 **Figure 5:** (Left) January observed SST, its difference (CONTROL-SMOOTH), and the difference
 475 (CONTROL-SMOOTH) in storm tracks over the North Pacific Ocean. The thin black contours show $\overline{v'T'}$ from
 476 the CONTROL case. The 95% confidence level is demonstrated by thick contours. (Right) As in (left) but for
 477 over the North Atlantic. Black contours in (f) denote Eady growth rate at 775hPa. The dashed and solid blue
 478 contours indicate significant differences at the 10 and 5% levels, respectively. Figures adapted from Kuwano-
 479 Yoshida and Minobe (2017) and O'Reilly et al. (2016, 2017).
 480

481 To better elucidate the forcing of near-surface weather by the oceans, other studies define the
 482 surface storm track as the variance of near-surface meridional winds (Booth et al. 2010, 2017;
 483 O'Neill et al. 2017; Small et al. 2019). The concept of the surface storm track stems from earlier
 484 scatterometer measurements illustrating a strong imprint of the free-tropospheric storm tracks in
 485 the surface wind fields over the warm WBCs (Sampe and Xie 2007; Bourassa et al. 2013). The
 486 reduced static stability and the induced vertical mixing within the MABL lead to the co-location

487 of the surface storm track with the warm currents. The surface and free-tropospheric storm tracks
488 are thus dynamically coupled via deep moist convection (Czaja and Blunt 2011).

489

490 Recent studies indicate that atmospheric mesoscale phenomena, such as atmospheric fronts,
491 within the storm tracks strongly interact with the WBC fronts. Parfitt and Czaja (2016) used
492 reanalysis data over the Gulf Stream, and Parfitt et al. (2016) used AGCM simulations over the
493 KOE to argue that the cross-frontal sensible heat flux gradients across the SST fronts exert
494 "thermal damping or strengthening" of atmospheric fronts depending on the space-time
495 alignment between the SST gradients and atmospheric fronts. The dominant cross-frontal length-
496 scale of the atmospheric fronts is comparable to that of the WBC SST fronts, enabling such
497 direct scale-to-scale thermal exchanges between the SST fronts and atmospheric fronts. The most
498 significant diabatic heating by surface fluxes is concentrated on the narrow space-time scales at
499 which the cold sectors of the atmospheric front coincide with the warm sector of the SST fronts.

500

501 Other studies emphasize the limited role of SST fronts on extreme cyclones. Masunaga et al.
502 (2020a,b) showed that storms and fronts of moderate-intensity are significant contributors to the
503 time-mean convergence observed over the Gulf Stream and KOE. AGCM experiments by
504 Tsopouridis et al. (2021) indicated that the direct impacts of sharp SST fronts on individual
505 cyclones over the Gulf Stream and KOE are weak, although SST fronts induce significant
506 indirect responses in large-scale environments in which storms form. Using an idealized analytic
507 model, Reeder et al. (2021) showed that diabatic frontogenesis over the WBCs could lead to
508 intensification of atmosphere fronts only when strong and rapidly propagating synoptic systems
509 are not already in the environment.

510

511 Much uncertainty still remains in model simulations and observational analysis regarding the
512 relative importance of SST gradients causing cross-atmospheric frontal sensible heat flux
513 gradients vs. absolute SST affecting the large-scale condensational heating over warm currents.
514 The nature of the forcing is key in assessing whether high-resolution climate models with sharp
515 SST fronts are necessary. The SST contribution to the precipitation from the warm and cold
516 sectors of extratropical cyclones differs in terms of magnitude and spatial distribution: larger and
517 broader for the warm sectors and weaker and more "anchored" to the SST fronts for the cold

518 sectors (Vannière et al. 2017). It is likely that the cold sector contribution has been dominating
519 the sensitivity of relatively high-resolution (~50 km) AGCM simulations to SST smoothing. It
520 remains an open question whether even higher resolution AGCMs might amplify a sensitivity
521 from the dynamics of the warm sectors, including mesoscale instabilities developing on the
522 warm conveyor belt (Czaja and Blunt 2011; Sheldon et al. 2017).

523

524 *c. Near-surface wind convergence over the WBCs*

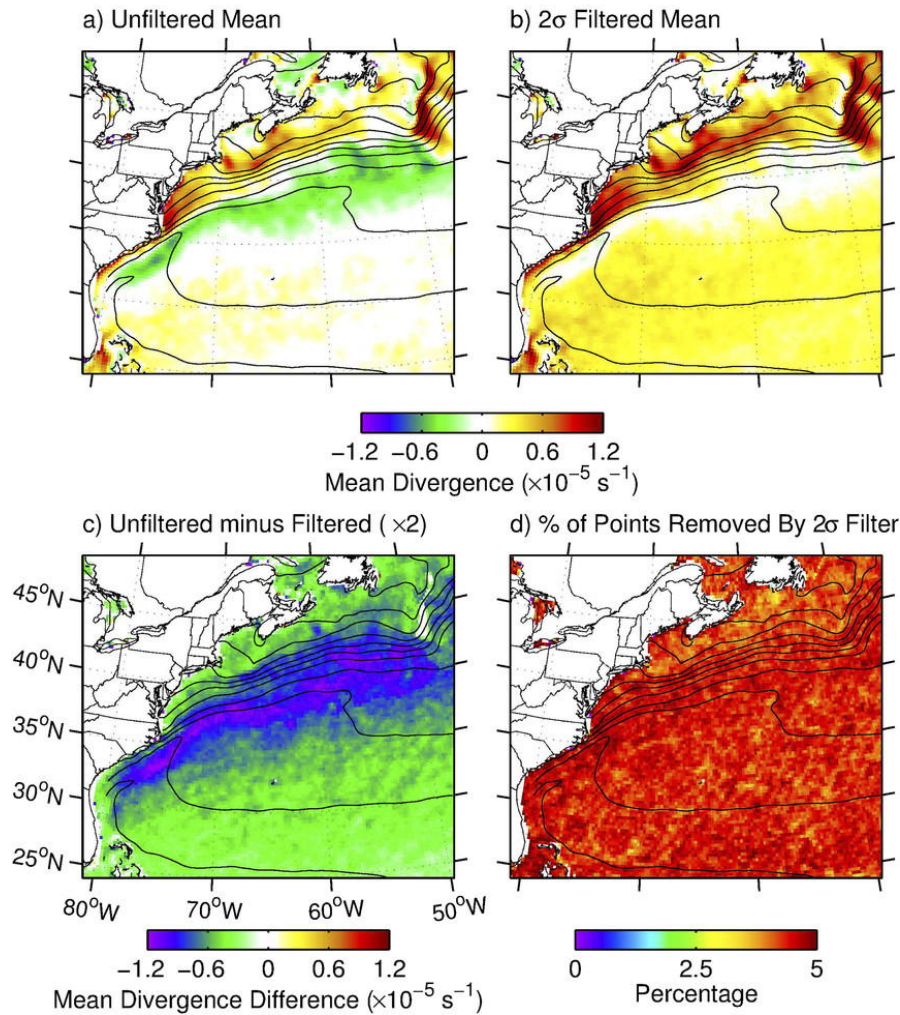
525 A crucial part of the storm track response to SST is precipitation, which tends to cluster around
526 the WBCs and is associated with high near-surface wind convergence (NSWC) and substantial
527 vertical ascent. The climatological NSWC is observed to coincide with the ocean fronts and the
528 Laplacians of SST and SLP, which indicates that the boundary layer process depicted by linear
529 Ekman dynamics is germane to the observed NSWC and precipitation responses (Feliks et al.
530 2004; Minobe et al. 2008, 2010). However, the unambiguous attribution of NSWC to the steady
531 Ekman-balanced mass adjustment mechanism is difficult due to the coexistence of extratropical
532 storm tracks with the WBC currents, which also induce minima in the time-mean SLP Laplacian
533 over the SST fronts (O'Neill et al. 2017).

534

535 O'Neill et al. (2015) show from QuikSCAT observations and a regional atmospheric model that
536 linear boundary layer dynamics cannot explain the daily time-scale occurrence of NSWC since,
537 on rain-free days, surface divergence dominates even though the SST Laplacian would indicate
538 convergence. Using an extreme value filter, O'Neill et al. (2017) further show that NSWC and
539 vertical motion over the Gulf Stream are highly skewed and consist of infrequent yet extreme
540 surface convergence events and more frequent but weak, divergent events, such that the median
541 surface flow field is weakly divergent or nearly non-convergent (Figure 6). Parfitt and Czaja
542 (2016) and Parfitt and Seo (2018) argue that much of the precipitation and NSWC are associated
543 with atmospheric fronts given that only a weak near-surface divergence remains in longer time
544 means when the contribution from atmospheric fronts is removed (Rousseau et al. 2021).

545

10-yr Mean All-Weather QuikSCAT Divergence



546

547 **Figure 6:** Maps of the 10-yr-mean QuikSCAT all-weather divergence (a) consisting of all points; (b) after
 548 application of the 2σ temporal extreme-value filter; (c) difference between (a) and (b); and (d) the percentage
 549 of divergence points removed by the 2σ extreme-value filter. The contours in each panel are of the 10-yr-mean
 550 Reynolds SST with a contour interval of 2°C . From O'Neill et al. (2017).
 551

552 Current research emphasizes identifying how and why atmospheric fronts align with and linger
 553 over ocean fronts in all major WBCs and whether there is an additional underlying, steady,
 554 small-scale boundary layer effect. For example, Small et al. (unpublished manuscript) argue for a
 555 distinct temporal dependence of the NSWC over WBC SSTs, where atmospheric fronts govern
 556 its day-to-day variability, while the pressure adjustment and vertical mixing mechanisms provide
 557 lower frequency modulations. This is consistent with the results from Brachet et al. (2012), who
 558 separate the SLP Laplacian into sub-10 day and longer time-scales, showing the former being
 559 dominated by the synoptic disturbances and the latter the SST forcing.

560 *d. Large-scale/downstream atmospheric circulation responses*

561 Many AGCM studies demonstrate a non-local, downstream response in the storm track to WBC
562 SST forcing. Wills et al. (2016) identified significant transient atmospheric circulation responses
563 downstream that lag the SSTA in the Gulf Stream extension by several weeks. O'Reilly et al.
564 (2016, 2017) found the northward shifted eddy-driven jet and the increased European blocking
565 frequency in response to a strengthened storm track over the Gulf Stream. Along a similar line,
566 Lee et al. (2018) suggested that SST biases near the Gulf Stream trigger extended biases in the
567 simulation of deep convection and downstream circulation via Rossby wave response.

568

569 Similarly, O'Reilly and Czaja (2015) found that when the KOE front is in its stable regime
570 featuring increased SST gradients, baroclinic eddies grow faster. The local shift in baroclinic
571 wave activity leads to the early barotropitization of the baroclinic eddies downstream, resulting
572 in weaker poleward eddy heat flux and increased occurrence of blocking in the eastern Pacific.
573 An AGCM study by Kuwano-Yoshida and Minobe (2017) also suggested the enhanced storm
574 track by the KOE SST fronts leads to a northward shifted storm track in the eastern Pacific. By
575 considering only the transient SSTA due to KOE mesoscale eddies, Ma et al. (2015, 2017)
576 showed that a northward shifted storm track led to reduced precipitation in parts of western
577 North America during the eddy-active KOE years (Foussard al. 2019b; Liu et al. 2021; Siqueira
578 et al. 2021). In the Southern Ocean, Reason (2001) showed that amplified cyclone activity over
579 the warm Agulhas Current yielded an enhanced storm track in the southeast Indian Ocean.

580

581 *e. Climate change*

582 Climate change simulations for the 21st Century have emphasized the critical role of ocean
583 circulation leading to natural modes of variability such as ENSO and PDO (Seager et al. 2001),
584 the predicted weakening of the Atlantic Meridional Overturning Circulation (AMOC; Weaver et
585 al. 2012), and the delayed warming of the Southern Ocean (Marshall et al. 2014). These changes
586 are relevant to a predicted intensification and poleward shift of the Kuroshio and Agulhas,
587 weakening of the Gulf Stream, and changes in the frontal systems of the Antarctic Circumpolar
588 Current (ACC) (e.g., Yang et al. 2016).

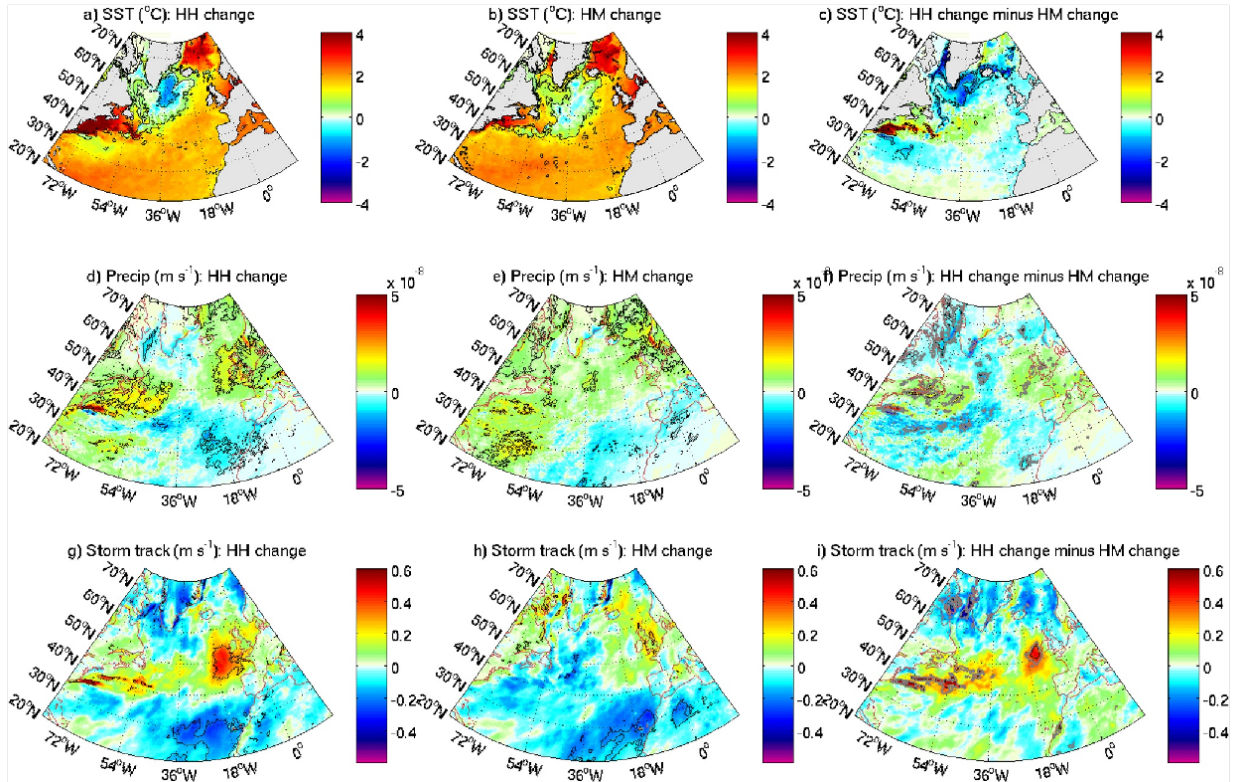
589

590 The IPCC report (IPCC, 2021) indicates that during the 21st Century, the North Pacific storm
591 track will most likely shift poleward, the North Atlantic storm track is unlikely to have a simple
592 poleward shift, and the Southern Hemisphere storm track will likely shift poleward.

593 Understanding these regional differences in projected changes in midlatitude storm tracks and
594 precipitation and their association with the predicted WBC changes have been the primary goals
595 of high-resolution CGCM studies, especially those that contrast the CGCMs with eddy-rich
596 ocean (typically 0.1° resolution) to those with eddy-parameterized ocean (0.5-1°). These studies
597 with increased ocean model resolution to mitigate the known biases in representing the WBC
598 dynamics and separation show distinct responses in SSTs and storm tracks in the WBC regions
599 in response to anthropogenic climate change.

600
601 The Kuroshio front in the eddy-rich simulations shifted equatorward, contrary to projections by
602 the IPCC-class CGCMs, which likely reflects the large natural variability in the North Pacific
603 (Taguchi et al. 2007; Seager and Simpson 2016). In the North Atlantic, the Gulf Stream
604 separation tends to be too far north in lower resolution models, but is improved in eddy-rich
605 models. This makes it possible for the separation to move northwards as a response to AMOC
606 weakening in eddy-rich models (Gervais et al. 2018; Moreno-Chamarro et al. 2021; Grist et al.
607 2021), leading to a significant projected ocean warming near the US eastern coastline (Figure 7;
608 Karmalkar and Horton 2021). In the Southern Ocean, CMIP5-based climate change simulations
609 indicate delayed warming, which is often attributed to stratospheric ozone depletion
610 (McLandress et al. 2011; Polvani et al. 2011). However, the recent satellite observations and
611 eddy-rich CGCMs simulations indicate a ubiquitous cooling trend (1961-2005) poleward of the
612 ACC due to resolved ocean eddies (Bilgen and Kirtman 2020). Analysis of eddy-rich ocean
613 simulations also indicates warmer and stronger Southern Hemisphere WBCs, suggesting that
614 resolved ocean eddies play a critical role in long-term SST changes.

615



616

617

618

619

620

621

622

Figure 7: (a-c) 2031–2050 minus 1951–1970 differences simulated by the HadGEM3-GC3.1, with 25 km atmospheric resolution coupled to 1/4° ocean (eddy-permitting, HM) and 1/12° ocean (eddy-rich, HH): SST (°C) (a) HH and (b) HM, precipitation (m s^{-1}) (d) HH and (e) HM; surface storm track (m s^{-1}) (g) HH and (h) HM. Panels (c, f, i) show the difference between the HH future change and the HM change. The black lines denote the 95% significance. Gray lines in (c,f,i) denote the 90% significance. From Grist et al. (2021).

623

624

625

626

627

628

629

630

631

632

633

634

635

The reorganization of the oceanic frontal zone and its associated eddy field modulates the low-level baroclinicity (Dacre and Gray 2013) and the strength and location of the diabatic heating source for the atmosphere. It is clear from this and other studies (Woollings et al. 2012; Winton et al. 2013; Keil et al. 2020) that such features would not occur in the absence of ocean circulation changes. However, the exact pattern of large-scale SST change is highly dependent on the ocean model and its resolution (Saba et al. 2016; Menary et al. 2018; Alexander et al. 2020), which also affects the projected WBC responses to climate change (Jackson et al. 2020). The climate projections with eddy-rich oceans have typically been performed with a small number of realizations and relatively short durations due to high computational cost (e.g., Haarsma et al. 2016). Currently, high-resolution coupled climate modeling projects are underway with much longer integration and multi-ensembles (e.g., Chang et al. 2020; Wengel et al. 2021). These efforts will enable a robust assessment of the forced responses in WBC and ocean circulation from natural variability in response to projected changes in the large-scale climate.

636 **4. Feedback of atmospheric mesoscale responses onto the ocean**

637 The new insights gained from these studies have led to improved process understanding and
638 notable revisions of theories of ocean circulation. This section discusses current knowledge of
639 ocean feedback mechanisms, feedback impacts on ocean biogeochemical cycles, and theories of
640 ocean circulation and model parameterizations to account for eddy-atmosphere interaction.

641

642 *a. Feedback to ocean circulation*

643 For simplicity, we consider two categories of oceanic mesoscale effects on air-sea fluxes: SST
644 impacts (thermal) described in Section 2b1, and surface current impacts (mechanical) in Section
645 2b2. The thermal feedback (TFB) results from kinematic and thermodynamic responses in the
646 MABL to mesoscale SSTs, modifying the wind stress and heat fluxes. The current feedback
647 (CFB) represents the processes by which the surface ocean current alters the wind stress, near-
648 surface wind, and turbulent heat fluxes, and thereby ocean circulation.

649

650 1) Thermal feedback (TFB) effect

651 Observed near-surface wind stress responses to mesoscale processes by Chelton et al. (2004)
652 were largely based on the TFB effect. Vecchi et al. (2004) and Chelton et al. (2007)
653 hypothesized that the wind stress curl responses to SST fronts would constitute an important
654 feedback mechanism driving ocean dynamics. Spall (2007) considered the impacts of SST-
655 induced Ekman pumping on baroclinic instability in the modified linear theory by Eady (1949),
656 showing that the SST-induced Ekman pumping adjusts the growth rate and wavelength of the
657 most unstable waves, especially the low-latitude flows with strong stratification. Hogg et al.
658 (2009) extended SST-induced Ekman pumping to an idealized double-gyre circulation in mid-
659 latitudes, showing that it destabilizes the eastward jet with the enhanced cross-gyre potential
660 vorticity fluxes, stabilizing the double gyre circulation by 30-40%.

661

662 Mesoscale SSTAs are damped by induced turbulent heat fluxes (THF), resulting in a negative
663 SST-THF correlation at mesoscales (Figure 1b-c). Over the KOE, Ma et al. (2016) examined this
664 mesoscale SSTA damping in the context of eddy potential energy (EPE) budget and the Lorentz
665 energy cycle. Compared to the eddy-filtered coupled model simulation (using a 1000 km-by-
666 1000 km boxcar filter), the eddy-unfiltered simulations showed a significant increase (>70%)

667 diabatic EPE dissipation, leading to a decrease of EKE by 20-40%, most strongly at wavelengths
668 shorter than 100 km. Other studies find that TFB has a weak impact on EKE (Seo et al. 2016;
669 Seo 2017). The cause of this discrepancy is partially due to different filter cutoffs used to define
670 the eddies. Renault et al. (unpublished manuscript) show that a large filter cutoff, as used in Ma
671 et al. (2016), overestimates EKE damping and may also smooth large-scale meridional SST
672 gradients, altering the large-scale wind curl and the mean oceanic circulation. Bishop et al.
673 (2020) evaluated the EPE damping over the global oceans using eddy-resolving climate model
674 simulations to find that the diabatic EPE damping was stronger over warm-core eddies.

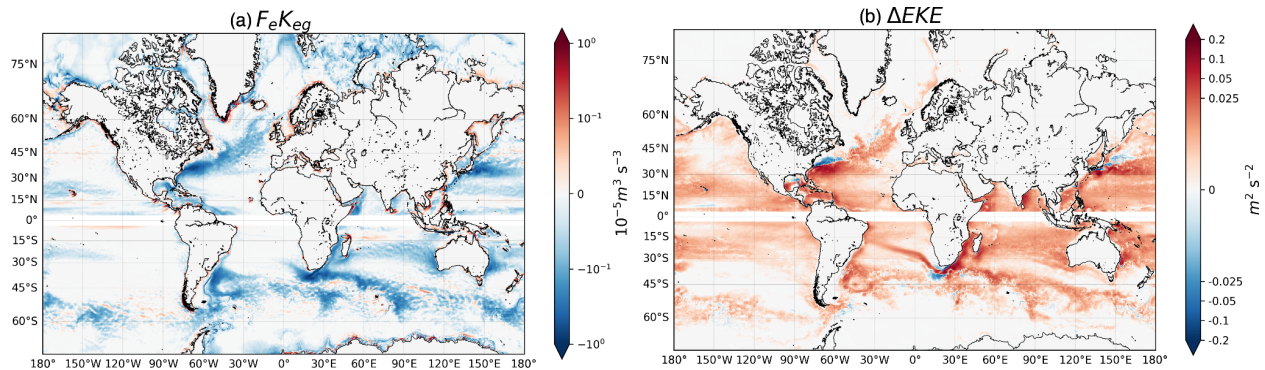
675

676 2) Current feedback (CFB) effect

677 Surface currents, although weaker than surface winds, modify surface stress directly by altering
678 wind speed (Bye 1986). In turn, by modulating the stress, the CFB exerts a "bottom-up" effect on
679 the wind, where a positive current anomaly causes a positive wind anomaly via a negative stress
680 anomaly (Renault et al. 2016a; 2019a). The CFB effect has initially focused on impact on wind
681 stress. Using satellite and in situ data, Kelly et al. (2001) showed that CFB reduces the median
682 wind stress from 20% to 50% near the equator, and Chelton et al. (2004) observed a clear imprint
683 of the Gulf Stream flow on the surface stress and the curl.

684

685 Several studies have highlighted the role of CFB as a "top drag" (Dewar and Flierl 1987), acting
686 on the oceanic circulation over a wide range of space-time scales. At the large-scale where the
687 currents tend to flow downwind, CFB reduces the mean input of energy from the atmosphere to
688 the ocean and therefore slows down the mean circulation (Pacanowski et al. 1997). By
689 weakening net energy input to the ocean, CFB triggers a host of changes in eddy-mean flow
690 interactions and the inverse cascade of energy, weakening baroclinic and barotropic instabilities
691 and the mesoscale activity (Renault et al. 2017b, 2019a; Figure 8). When the wind and current
692 are in the opposite sense, the CFB serves as a conduit of energy from the ocean to the
693 atmosphere, which can be seen from satellite data as negative mean and eddy wind work (Figure
694 8a; Scott and Xu 2009; Renault et al. 2016a,b, 2017a). Numerous studies have demonstrated a
695 strong EKE damping effect of ~30% (See references in Jullien et al. 2020; Figure 8b). CFB also
696 induces additional Ekman pumping that weakens an eddy (Gaube et al. 2015) and influences the
697 upper-ocean stratification (Seo et al. 2019; Song et al. 2020).



699

700 **Figure 8:** (a) Geostrophic eddy wind work ($10^{-5} \text{ m}^3 \text{ s}^{-3}$) estimated from the EC-Earth global coupled simulation
 701 with current feedback (CFB). The negative values indicate a transfer of momentum from geostrophic
 702 mesoscale currents to the atmosphere. This sink of energy is the main driver of the damping of EKE illustrated
 703 in (b), as illustrated by the difference of EKE ($\text{m}^2 \text{ s}^{-2}$) between simulations without CFB and with CFB. Both
 704 wind work and EKE are estimated over a 30-yr. period. Details about the coupled model and experiments can
 705 be found in Renault et al. (unpublished manuscript).

706

707 The role of CFB in ocean circulation modifies the classic concept of wind-driven currents. While
 708 the wind remains a large-scale energy source that initiates a turbulent cascade, its fine-scale
 709 interactions with currents also affect the entire oceanic spectrum. The route to dissipation in the
 710 ocean is still an open question. However, recent findings point to the role of mesoscale air-sea
 711 coupling via ocean currents that offers an unambiguous sink of energy to achieve proper
 712 equilibrium in ocean dynamics (Renault et al. 2016a; Fox-Kemper et al. 2019). Recent studies
 713 also have emphasized the CFB impact on near-surface winds (Renault et al. 2016a, 2017a,
 714 2019a), which has led to an effort to accurately represent the CFB effect on air-sea momentum
 715 exchanges in ocean-only models. Renault et al. (2020) tested new parameterizations that correct
 716 wind stress based on these coupling coefficients predicted from the wind magnitude, allowing
 717 replication of both wind and stress responses to CFB and the level of eddy energy from coupled
 718 simulations. As an indirect effect, CFB also exerts a strong control on WBC dynamics by
 719 weakening the inverse cascade of energy (Renault et al. 2019b).

720

721 There are a few remaining unknowns. First, little is known about CFB at the submesoscale. For
 722 the US West Coast, Renault et al. (2018) highlighted a submesoscale dual effect of CFB: it
 723 damps submesoscale eddies but also catalyzes submesoscale current generation. By affecting
 724 mixing, stratification, and eddy variability, CFB will modulate biogeochemical variability
 725 (McGillicuddy et al. 2007; Kwak et al. 2021). Since CFB and TFB coexist where mesoscale

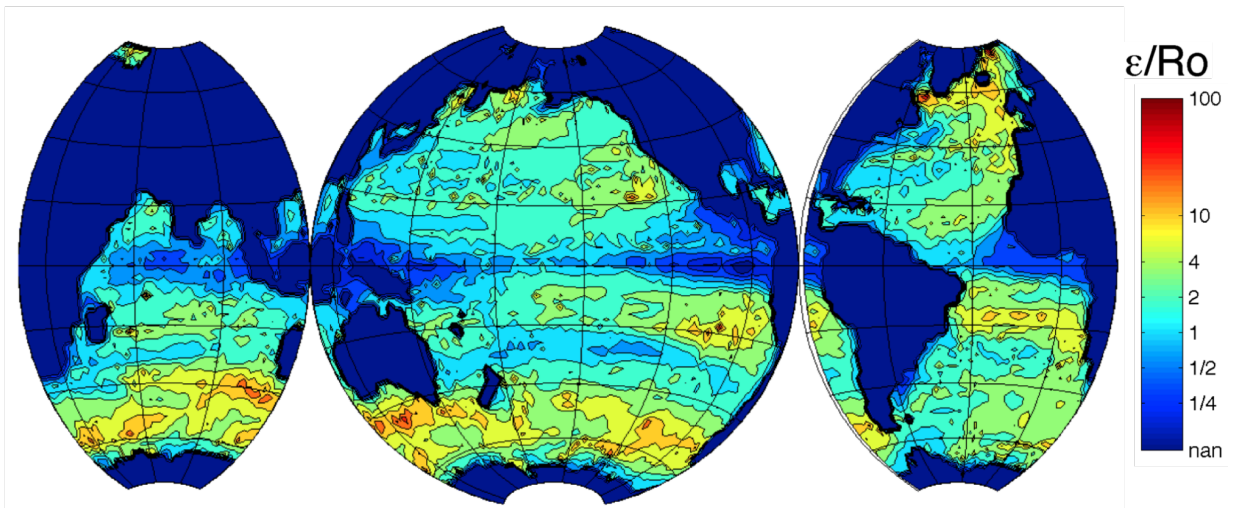
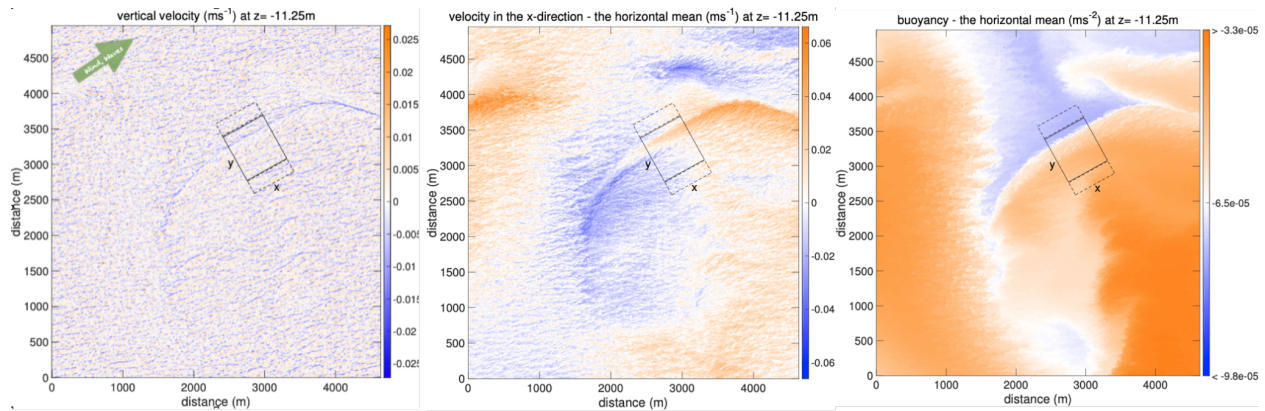
726 currents are strong (Song et al. 2006; Seo et al. 2007; Takatama and Schneider 2017; Renault et
727 al. 2019b; Shi and Bourassa 2019), CFB likely influences large-scale boundary-layer moisture,
728 clouds, precipitation, and atmospheric circulation via rectified effects. However, this downstream
729 influence is only beginning to be explored (e.g., Seo et al. 2021). Finally, in the areas of strong
730 tidal variability, tidal currents can exceed wind speed; whether the tidal current effect will be
731 averaged out or whether it exerts a low-frequency rectified effect is an open question.

732

733 *b. Impact of surface waves*

734 While sea state is a salient aspect of air-sea fluxes (Fairall et al. 1996; Cavaleri et al. 2012; Edson
735 et al. 2013), other aspects of wave interactions with (sub)mesoscale currents may be important
736 for air-sea fluxes and regional circulation. It has long been known that sheared currents affect the
737 propagation of surface wave rays (Villas Bôas and Young 2020). In the open ocean, the spatial
738 gradients in mesoscale surface currents dominate the variability of significant wave height,
739 leading to the refraction of waves near steep vorticity gradients (Ardhuin et al. 2017; Villas Bôas
740 et al. 2020). Similarly, the underpinnings of the Craik-Leibovich theory of Langmuir turbulence
741 specify that rectification of wave-vorticity interactions in the upper ocean leads to Stokes forces,
742 which can cause substantial wave effects on currents (Leibovich et al. 1983; Lane et al. 2007).
743 LES models that include vortex forces and regional models that include the wave refraction by
744 currents (Romero et al. 2020) illustrate the frontal adjustment and frontogenesis triggered or
745 enhanced by surface wave interactions (McWilliams and Fox-Kemper 2013; Suzuki et al. 2016;
746 Sullivan and McWilliams 2019). Examples are provided in Figure 9 (upper panel), where a
747 submesoscale density front in the downwind and down-Stokes direction interacts with Langmuir
748 turbulence. Strong overturning circulation (downwelling) sharpens the front and strengthens the
749 along-front jet. Classic balances are altered by waves to yield the wavy Ekman balance
750 (McWilliams et al. 2012), the wavy geostrophic balance (McWilliams and Fox-Kemper 2013,
751 Figure 9, lower panel), and the baroclinic and symmetric instabilities affected by waves (Haney
752 et al. 2015).

753



754 **Figure 9:** (Upper panel) Examples of a front interacting with Langmuir turbulence (box centered on this
 755 feature), which is aligned in the downwind and down-Stokes direction. (Left) vertical velocity showing
 756 ubiquitous Langmuir cells, but also a long, coherent (downwelling) overturning circulation along the front due
 757 to frontogenesis and accelerated by the Stokes shear force. (Center) Along-front (x-direction) velocity shows
 758 the frontal flow. (Right) The front is characterized by a sharp transition in buoyancy (or temperature). Adapted
 759 from Suzuki et al. (2016). (lower panel) Estimated ratio of ϵ (strength of Stokes drift-induced vertical
 760 acceleration vs. buoyancy, an indicator of wave contributions added to the traditional hydrostatic balance) to
 761 Rossby number (indicating geostrophic balance). This ratio implies the deviation from hydrostatic balance due
 762 to waves as compared to the deviation from geostrophic balance due to advection. This estimate is based on the
 763 de Boyer-Montegut et al. (2004) mixed layer depth climatology (h) and a global simulation of WaveWatch3,
 764 and AVISO geostrophic velocity. Figures redrawn from McWilliams and Fox-Kemper (2013).
 765
 766

767 However, these studies of wave-induced mixing, frontogenesis, and instability do not yet fully
 768 take into account the impact of wave growth and breaking by the wind that is correlated with
 769 mesoscale SST gradients or ocean currents. Since both wave effects on currents and current
 770 effects on waves would strengthen as the fronts become smaller and more intense, emerging
 771 high-resolution fully-coupled model simulations that resolve fine-scale flow fields in the ocean
 772 are expected to represent this wave-current interaction better (Haney et al. 2015; Romero et al.
 773 2020). The significance of these effects suggested by such models will motivate simultaneous

774 observations of waves, currents, and air-sea fluxes to guide revised theories of wave-current
775 interaction and validate high-resolution model simulations.

776

777 *c. Ocean model physics*

778 Traditionally, mesoscale and submesoscale eddy parameterizations have been deterministic and
779 have focused only on effects on the mean and variance of tracers (Gent and McWilliams 1990;
780 Fox-Kemper et al. 2011), while neglecting rectified effects on air-sea coupling. However, in
781 simulations where some eddies are resolved, deterministic closures do not stimulate a resolved
782 eddy response or backscatter (e.g., Bachman et al. 2020). In response, there is a growing
783 desire to implement stochastic parameterizations of the eddy transport into non-eddy-resolving
784 models, for example, via uncertainty in location (Memin 2014), transport (Drivas et al. 2020),
785 closure (Nadiga 2008; Jansen and Held 2014; Zanna et al. 2017; Bachman et al. 2020), or
786 equation of state (Brankart 2013). This can potentially include stochastic parameterizations of
787 the air-sea coupling simultaneously. As stratification and rotation parameters vary globally,
788 building scale awareness into parameterizations is also crucial (Hallberg 2013; Dong et al. 2020,
789 2021). Observed air-sea fluxes are highly variable, indicating a response to high spatio-temporal
790 variability (Yu 2019), scale dependence (Bishop et al. 2017, 2020), sea state dependence
791 (Kudryavtsev et al. 2014), and thus offering the potential for stochastic implementation. While
792 idealized studies have begun to develop a process-level understanding (Sullivan et al. 2020,
793 2021), at the time of this review, no realistic model implementation of stochastic air-sea fluxes
794 seems to have been evaluated carefully.

795

796 *d. Impacts on primary productivity*

797 Mesoscale air-sea interaction can also influence biogeochemical environments and hence
798 primary productivity (e.g., McGillicuddy 2016). The wind stress response to mesoscale SST and
799 currents introduces perturbation Ekman upwelling and downwelling, leading to, for example,
800 dramatic mid-ocean mesoscale plankton blooms in the nutrient-replete subtropics (McGillicuddy
801 et al. 2007). Global satellite-based eddy-composite analyses demonstrate the widespread effect
802 of mesoscale air-sea interaction on the ocean biogeochemical environment via eddy currents and
803 SST (e.g., Gaube et al. 2015). Additionally, eddy-induced modifications of wind stress impact
804 vertical mixing in the upper oceans. Eddy effects on mixed-layer depths are asymmetric between

805 anticyclones and cyclones (e.g., Dufois et al. 2017; Hausmann et al. 2017). However, to what
806 extent this asymmetry stems from the mesoscale modulations of surface wind stress has yet to be
807 determined. Considering the prevalence and persistence of nonlinear mesoscale eddies in the
808 global oceans (Chelton et al. 2011a,b), the relevance of mesoscale eddy impacts on primary
809 productivity via eddy-wind interaction needs robust quantification.

810

811 **5. State of observational capabilities**

812 Observing mesoscale air-sea interaction processes is challenging since multiple oceanic and
813 atmospheric parameters must be measured with high accuracy and spatio-temporal resolution.
814 The past decade has seen the emergence of novel in situ and remote sensing platforms that will
815 increasingly better capture mesoscale and smaller processes with high accuracy and resolution
816 (e.g., Chapter 9 of Kessler et al. 2019). Here, we briefly discuss the existing and novel
817 observational technologies that can provide multi-platform, coordinated measurements for air-
818 sea interaction studies (e.g., Bony et al. 2017; Wang et al. 2018).

819

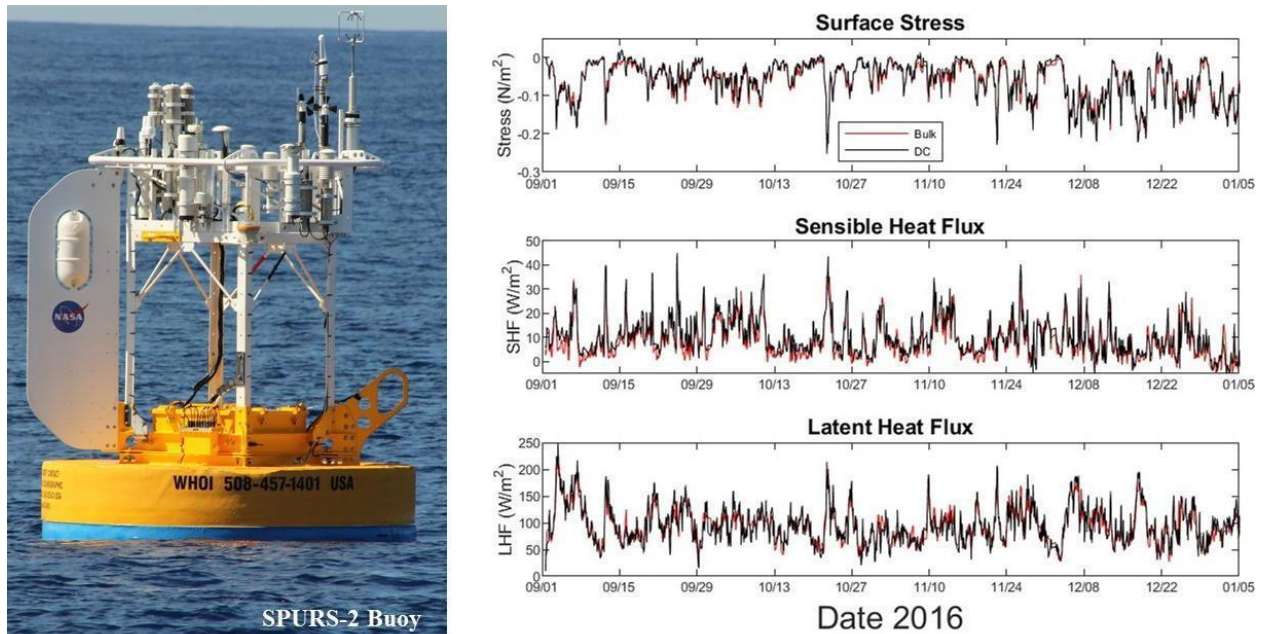
820 *a. In situ observations*

821 Oceanographic moorings can be equipped with meteorological instruments, including direct
822 covariance flux system and bulk meteorological sensors to provide the directly measured and
823 bulk-estimated air-sea fluxes, respectively. An example system is shown in Figure 10 from the
824 second Salinity Processes in the Upper-ocean Regional Study (SPURS-2) experiment, which
825 computed and telemetered in near-real-time the motion-corrected surface wind stress and
826 sensible and latent heat fluxes from a surface mooring for the first time (Clayson et al. 2019).
827 Recently, buoy arrays have been deployed as part of the Ocean Observatories Initiative (OOI,
828 Trowbridge et al. 2019) and operated for years on both coasts. These data, along with the
829 simultaneous measurements of surface meteorology and wave conditions, are crucial to reducing
830 the uncertainty in air-sea flux estimates in modern bulk formulas (Cronin et al. 2019).

831 Autonomous surface vehicles (ASVs) are piloted wave- or wind-propelled surface platforms that
832 can be instrumented with ocean, atmospheric, and biogeochemical sensors. Widely-used ASVs
833 include Saildrone (Meinig et al. 2019) and Wave Gliders (Thomson and Girton 2017), which
834 have long endurance (~6 months) and can sample in remote locations and be piloted across
835 fronts. The use of numerous instruments can mitigate issues with cross-frontal sampling and can

836 thus capture mesoscale and smaller variations in air-sea interaction (Quinn et al. 2021; Stevens et
837 al. 2021).

838



839 **Figure 10:** (left) The SPURS-2 central mooring with instrumentation at the upper right includes a sonic
840 anemometer, infrared hygrometer, and sensors to remove buoy motion. The sensor package can directly
841 measure the surface stress, sensible heat, and latent heat fluxes. (right) Time series of these fluxes showing
842 bulk estimates in red and direct covariance (DC) fluxes in black. Good agreement is seen between the bulk and
843 DC estimates, with the most significant discrepancies visible in the sensible heat flux. Photo by James B.
844 Edson (WHOI).
845

846

847 Drifting platforms can be instrumented with a variety of sensors that capture air-sea interaction.
848 The Global Drifter Program, a global network of surface drifters that typically measure currents,
849 SST, and barometric pressure, has contributed to the understanding of global mesoscale
850 circulation (Laurindo et al. 2017; Centurioni et al. 2019). Drifting spar buoys (Graber et al. 2000;
851 Edson et al. 2013) have been used to measure surface fluxes in situ for decades. In recent years,
852 sophisticated low-profile Lagrangian platforms have been developed such as SWIFTs (Thomson
853 2012) to measure surface currents, waves, and near-surface ocean turbulence over a range of
854 wave conditions. Benefits of drifters include relatively low cost and Lagrangian sampling.
855 However, they tend to converge at fronts and therefore multiple drifters are necessary to
856 characterize cross-frontal structure (D'Asaro et al. 2018).

857

858 Aircraft measurements have also been important for air-sea interaction studies. The mobility of
859 the platform is advantageous because of its ability to obtain in situ measurements of the
860 horizontal and vertical variability in and above the MABL in a short time. With carefully
861 designed flight patterns, it can also derive mesoscale forcing to the boundary layer using the
862 velocity field measured at flight level (Lenschow et al. 1999; Stevens et al. 2003). In the past 20
863 years, air-deployable sensor packages such as GPS dropsondes, AXBT, AXCTD, and
864 instrumented floats have further expanded the sampling capability to depict the entire column of
865 the atmosphere and the upper ocean, particularly when low-level flights are not feasible (Doyle
866 et al. 2017). In recent years, airborne measurements have been extended down to 10 m above the
867 sea surface using a controlled towed vehicle (Wang et al. 2018). This new capability is a
868 significant addition to air-sea interaction studies, particularly on surface flux parameterization.

869

870 *b. Remote sensing*

871 Emerging remote sensing platforms, including satellite, ground-based, or airborne
872 measurements, present promising means to estimate air-sea fluxes at ocean mesoscale and
873 smaller. Scatterometer and microwave measurements provide global views of ocean vector
874 winds and SST under all wind conditions at daily scales. However, under extreme conditions,
875 large uncertainty exists due to inconsistent in situ reference wind speeds from dropsondes and
876 moored buoys to calibrate satellite winds (e.g., Polverari et al. 2021). This also implies
877 uncertainties in modeling ocean drag and air-sea interaction. The virtual constellation of
878 scatterometers (Stoffelen et al. 2019) provides good temporal coverage of the extremes with now
879 7 scatterometers in space with revisits globally within 30 minutes or a few hours (Gade and
880 Stoffelen 2019). Future satellite observations will need to resolve synoptic variability under
881 strong wind and rain and increase the resolution of the vertical profiles within the MABL to
882 better estimate the relationship between the surface flux and flux profiles.

883

884 For momentum fluxes, key variables are surface winds and currents. In coastal regions, high-
885 frequency radar systems provide surface currents at $O(1)$ km resolution (Paduan and Washburn
886 2013; Kirincich et al. 2019), which can be used to infer surface wave conditions and wind stress
887 (e.g., Saviano et al. 2021). The airborne DopplerScatt system simultaneously captures surface
888 wind stress, waves, and currents (Wineteer et al. 2020) and is central to the Sub-Mesoscale

889 Ocean Dynamics Experiment (S-MODE; Farrar et al. 2020). Similar measurement concepts have
890 been proposed for new satellites (Villas Bôas et al. 2019), such as Harmony (López-Dekker et al.
891 2019), SeaStar (Gommenginger et al. 2019), and the Winds and Currents Mission (WaCM;
892 Bourassa et al. 2016; Wineteer et al. 2020). Notably, the Harmony satellite mission relies on dual
893 synthetic aperture radar (SAR) to measure surface roughness, enabling high-resolution detection
894 of ocean fronts even in the presence of clouds. An increase in computing power and expansion of
895 machine learning techniques (e.g., Wang et al. 2019) have the potential to improve the utility of
896 SAR for air-sea interaction studies. Surface waves are also important in momentum flux
897 estimates; new satellite missions such as CFOSAT (Chinese-French Oceanography Satellite)
898 simultaneously measuring waves and winds (Ardhuin et al. 2019) are expected to improve the
899 accuracy of the wind-speed and wave-based formulations in the modern flux bulk formula.
900 Satellite surface measurements of stress-equivalent winds more closely respond to stress than
901 wind (e.g., de Kloe et al. 2017). Given the persistent large-scale and mesoscale errors in NWP
902 reanalyses (Belmonte and Stoffelen 2019; Trindade et al. (2020), these new satellite observations
903 collocated with surface measurements of stress will be valuable for understanding stress-related
904 air-sea coupling and improving ocean modeling and marine forecasting (Bourassa et al. 2019).
905
906 For turbulent heat fluxes, current satellite remote sensing systems rely on bulk parameterizations
907 to represent net heat and gas fluxes (Bourassa et al. 2013; Cronin et al. 2019). Mesoscale air-sea
908 interaction studies will benefit significantly from a satellite mission that measures co-located,
909 small-scale state variables, including near-surface atmospheric temperature and humidity, SST,
910 and wind speed to provide estimates of turbulent heat fluxes (e.g., Gentemann et al. 2020). This
911 will also help validate the numerical models to lower the uncertainty in air-sea heat flux. As for
912 the gas exchanges, new satellite missions, such as the Ka-band Doppler scatterometer that will
913 simultaneously measure ocean vector winds, waves, and currents at 200 m spatial resolution, or
914 the SWOT altimeter mission that will observe the dynamic topography at small mesoscales and
915 can be combined with ocean color, will help elucidate the role of mesoscale air-sea interactions
916 in biological and biogeochemical cycles in the coming years.
917

918 **6. Summary and discussions**

919 Since the first global-scale surveys of the mesoscale air-sea interactions by Chelton et al. (2004)
920 and Xie (2004), our theoretical understanding and observational and modeling capabilities in the
921 past two decades have advanced significantly, leading to a substantial body of literature related
922 to mesoscale air-sea interaction. Our current scientific understanding indicates that mesoscale
923 eddies actively perturb the MABL via surface flux anomalies leading to dynamic and
924 thermodynamic adjustments (Section 2). The MABL response is communicated to the free
925 troposphere, especially over WBCs, influencing downstream development of weather and short-
926 term climate events (Section 3). The MABL response feeds back to the ocean circulation,
927 influencing WBC dynamics, air-sea gas exchanges, and nutrient distribution (Section 4). This
928 new knowledge has transformed our classical understanding of physical processes, leading to
929 notable revisions of the theories of oceanic and atmospheric circulation (Section 4). Our
930 observational capability is advancing rapidly to better characterize mesoscale air-sea interaction
931 (Section 5). However, numerous challenges must be overcome to diagnose, observe, and
932 simulate mesoscale air-sea interaction. Here is the notable list (non-exhaustive) of issues in
933 theory, observations, and modeling that we think deserve some further comments.

934

935 *a. Climate modeling and physical parameterizations*

936 Significant progress has been made in understanding results and uncertainties in climate models
937 of different complexity and resolutions mainly via coordinated modeling experiments with
938 resolutions at or beyond the ocean mesoscale and common sets of diagnostics. The CMIP6
939 HighResMIP protocol was a step in this direction (Haarsma et al. 2016). Analyses from a subset
940 of these models from the PRIMAVERA project (Bellucci et al. 2021) reveal model resolution
941 sensitivity (especially in the oceans) of the simulated regimes of air-sea interaction and climate
942 in the extratropics. For example, Moreton et al. (2021) show how modeled air-sea flux feedbacks
943 can be damped depending on the relative ocean-atmosphere resolutions and coupling methods,
944 emphasizing the need for understanding these numerical aspects and the bulk formula in flux
945 calculations (See also Jullien et al. 2020). Further advances in model resolution, for example,
946 DYAMOND (Stevens et al. 2019) and the planned HighResMIP2, together with programs such
947 as OASIS (Observing Air-Sea Interaction Strategy, <https://airseaobs.org>) that aims to bring
948 observations and models closer together, will build on these previous efforts and provide further

949 insights into the fidelity of modeled mesoscale air-sea interactions. Furthermore, in the ocean
950 and coupled models where the ocean eddies are not fully or only partially resolved, their rectified
951 effects on the air-sea heat and momentum fluxes are not currently parameterized. Various
952 stochastic representations of eddy transports are being tested and implemented (Section 4c),
953 which can potentially address this issue of low-frequency rectification effects by eddies on large-
954 scale climate via air-sea interaction (e.g., Siqueira and Kirtman 2016).

955

956 *b. Ocean biogeochemistry processes*

957 Estimates of air-sea gas exchange of tracers do not fully consider effects arising from ocean
958 mesoscale eddies and fronts. One issue is that the gas transfer velocity typically (i) does not
959 consider wind variations introduced by mesoscale air-sea interactions, and (ii) is based on wind
960 speed (e.g., Wanninkhof 1992), and hence only implicitly accounts for the sea state variations.
961 Ocean mesoscale features influence the sea state and wind speeds, which are not always in
962 equilibrium, so that local wind alone is insufficient to describe the wave impact on gas
963 exchanges. Studies with parameterizations that consider bubble-mediated gas exchanges due to
964 breaking waves (e.g., Frew et al. 2007; Deike and Melville 2018) reveal their significant
965 contribution to regionally-integrated CO₂ flux especially under midlatitude storm tracks (e.g.,
966 Reichl and Deike 2020). To more accurately represent the sea state influence modulated by
967 mesoscale processes in the transfer velocity-based flux parameterization (e.g., Fairall et al. 2011;
968 Edson et al. 2011), it is imperative to increase direct measurements of CO₂ flux (e.g., McGillis et
969 al. 2001) along with the coincident observations of wind, waves, solubility, and air-sea partial
970 CO₂ pressure differences.

971

972 Further, physical mesoscale air-sea interaction likely feeds back to ocean primary productivity
973 (see the reviews by Lévy 2008; McGillicuddy et al. 2016), thereby also affecting air-sea fluxes
974 and tracer concentrations in the ocean, such as carbon. Mesoscale eddies are observed
975 ubiquitously in the global oceans; however, their physical properties, and their relationships with
976 biogeochemical variables, vary widely by region (e.g., Chelton et al. 2011; Gaube et al. 2013,
977 2014). Future work should aim to identify the specific aspects of this regional variability that are
978 due to mesoscale air-sea interaction and subsequent impacts on upwelling and vertical mixing.

979

980 It remains unclear how important biogeochemical effects due to mesoscale air-sea interactions
981 are for the larger-scale air-sea fluxes, biogeochemical mixed-layer properties, or ocean interior.
982 Eddy-rich climate model simulations are one avenue to gain more insight into the relevance of
983 the complex coupling of ocean mesoscale features, biogeochemistry, and the atmosphere. Few
984 such simulations currently exist due to their computational expense (e.g., Harrison et al. 2018),
985 but we expect this to change in the coming years. In addition, dedicated field experiments and
986 process studies are critical to determining what aspects of mesoscale air-sea interactions need to
987 be considered and represented in non-eddy-resolving models.

988

989 *c. Submesoscale air-sea interaction*

990 The ocean submesoscale processes with length-scales smaller than ~ 10 km are essential for the
991 ocean energy cycle (Lorenz 1960), global heat balance (Su et al. 2018), and marine
992 biogeochemistry and ecosystems (Omand et al. 2015; Lévy et al. 2018). While the dynamics of
993 the submesoscale ocean instabilities are becoming better understood (e.g., Fox-Kemper et al.
994 2008; D’Asaro et al. 2011), their direct impact on the MABL and heat and carbon uptake by the
995 oceans (e.g., Johnson et al. 2016; Bachman et al. 2017; du Plessis et al. 2019) are not as well
996 understood. Thus far, only a few satellite-based studies provide direct observational evidence of
997 relative wind stress response to submesoscale SST fronts (e.g., Beal et al. 1997; Xie et al. 2010;
998 Gaube et al. 2019; Ayet et al. 2021), although in situ observational studies have long documented
999 such interactions in localized regions (e.g., Sweet et al. 1981; Friehe et al. 1991; Mahrt et al.
1000 2004). While results from high-resolution numerical simulations (e.g., LES) indicate SST-driven
1001 MABL dynamics (Skylingstad et al. 2007; Lambaert et al. 2013; Wenegrat and Arthur 2018;
1002 Lac et al. 2018; Sullivan et al. 2020, 2021), they also recognize the importance of advection and
1003 convective organization to characterize nonlinear MABL dynamics at the submesoscale. As for
1004 the oceanic impact, the ocean current feedback dominates the wind stress response at the
1005 submesoscale, which influences the submesoscale flow fields and ocean kinetic energy (Renault
1006 et al. 2018). Spatial variability in sea state and surface roughness are enhanced at the
1007 submesoscale, and hence wave-current interactions (e.g., Villas Bôas and Pizzo 2021) and wave-
1008 wind interactions (e.g., Deskos et al. 2021) are expected to be critical in determining wind stress,
1009 heat flux, and MABL variations (Ayet et al. 2021). Emerging in situ and satellite observations
1010 for near-surface processes (Section 5) should be combined with dedicated atmospheric and

1011 oceanic LES and high-resolution modeling studies for boundary layer turbulence to improve the
1012 physical understanding of air-sea interactions at the submesoscale.

1013

1014 *d. Climatological near-surface wind convergence*

1015 There are some remaining questions regarding the essential role of WBC SST forcing on the
1016 time-mean atmospheric state. The ongoing debates about the origin of the near-surface wind
1017 convergence (NSWC) and the maximum precipitation over WBCs are particularly relevant as
1018 they entail important implications pertinent to various aspects of the topics discussed in this
1019 article. That is, to assess whether or not the steady linear boundary layer dynamics accounts for
1020 the time-mean NSWC and vertical motion requires a detailed understanding of the modulation of
1021 boundary layer ageostrophic circulation by SST (Section 2). On the other hand, the demonstrated
1022 impacts of storms and atmospheric fronts on the NSWC require a careful examination of
1023 extratropical cyclogenesis modulated by the diabatic forcing over the ocean fronts (Section 3).
1024 Overall, any approach to quantifying the nature of the relationships between time-mean
1025 convergence and SST will need to robustly separate the small magnitude convergence predicted
1026 by linear boundary layer theory from the anomalous convergence induced by storm systems that
1027 are several orders of magnitude greater.

1028

1029 *e. Diagnostics for air-sea interactions*

1030 The debate about the role of SST fronts in the NSWC arises partly due to the lack of a robust
1031 process-based diagnostics and analytic framework to interpret the observed convergence
1032 patterns. The existing analytical model of Schneider and Qiu (2015) discussed in Section 2c
1033 offers a complete account of the role of boundary layer dynamics over the SST fronts, which
1034 provides the two limiting cases of wind response to SST dependent on background wind speed.
1035 The model also suggests an extension of the diagnostic framework from the widely used
1036 coupling coefficients to lagged regression, impulse response, or corresponding spectral transfer
1037 functions. Yet, the model assumes a quasi-steady state and does not account for the processes
1038 associated with the storm tracks and their synoptic-scale influence on NSWC. A critical path
1039 forward is to incorporate the time-dependent or stochastic processes related to storms along SST
1040 frontal zones and the local SST-induced boundary layer response in a single analytical
1041 framework. Given the coexistence of the SST and current feedback effects along the frontal

1042 zones, such diagnostic frameworks will also have to consider the mechanical coupling effects
1043 simultaneously along with the thermal effects (e.g., Takatama and Schneider 2017).

1044

1045 *f. Downstream atmospheric circulation responses*

1046 Despite numerous studies suggesting WBC impacts on downstream atmospheric circulation, the
1047 nature of the far-field circulation response to WBC SST forcing and its statistical significance
1048 remains uncertain (Kushnir et al. 2002; Kwon et al. 2010; Czaja et al. 2019). Some studies argue
1049 that the sharpness of WBC fronts shifts the storm track and jet stream, influencing the blocking
1050 frequency in Europe and Northeastern Pacific (e.g., Kuwano-Yoshida and Minobe 2017;
1051 O'Reilly et al. 2015, 2016, 2017; Piazza et al. 2016). Other studies find that meridional shifts of
1052 WBC fronts alter the basin-scale transient eddy heat flux (e.g., Frankignoul et al. 2011; Kwon
1053 and Joyce 2013; Seo et al. 2017). Warm-core eddies near the KOE act as significant oceanic
1054 sources of moisture and heat for large-scale circulation, altering downstream precipitation
1055 patterns (Ma et al. 2015, 2016; Liu et al. 2021). Deriving a robust conclusion on downstream
1056 influences from these studies remains difficult since they adopt different methods to define WBC
1057 SST impacts, leading to distinct amplitudes/patterns of SST perturbations, and thus different
1058 atmospheric responses (this uncertainty is in addition to differences in model climatologies).
1059 Large-scale circulation will likely respond differently to different aspects of WBC SST
1060 variability. To date, the relative impacts of sharpness of SST gradient, its meridional shift, and
1061 activity of warm or cold-core eddies remain unquantified. The coordinated multi-model,
1062 common-forcing simulation and diagnostic framework, akin to PRIMAVERA/HighResMIP
1063 (Section 6a), will be extremely valuable in this regard, particularly with large ensemble sizes and
1064 long integrations to produce statistical robustness.

1065

1066 *g. Final remarks*

1067 Prospects for significant advances in mesoscale air-sea interaction in the coming years are
1068 extremely bright. Currently, strong community efforts and enthusiasm exist for building
1069 sustained observational networks to characterize detailed physical and biogeochemical processes
1070 across the air-sea coupled boundary layers (e.g., OceanObs'19 White Papers; OASIS). New
1071 satellite missions with advanced instrument technology and retrieval algorithms continue to be
1072 developed to improve our capability to monitor state variables pertinent to air-sea interactions at

1073 fine scales and high accuracy. These new observations lead to updated physical
1074 parameterizations that are increasingly more scale-aware and potentially built with stochastic
1075 schemes that account for rectified effects of eddy transports on air-sea flux and large-scales.
1076 More field experiments are being designed with close integration with process-oriented and data
1077 assimilative modeling to help not only design the sampling plans but also improve the
1078 parameterizations and skills in prediction models (e.g., Cronin et al. 2009; Cravatte et al. 2016;
1079 Kessler et al. 2019; Sprintall et al. 2020; Shroyer et al. 2021; Shinoda et al. 2021). The climate
1080 modeling community is developing and refining high-resolution Earth system model simulations
1081 with advanced physical parametrizations. International partnership and coordination are
1082 becoming ever more solid, enabling the design of multi-model, multi-ensemble, high-resolution
1083 coupled modeling protocols and diagnostic frameworks. The identified common biases in
1084 mesoscale air-sea interaction in such climate models, in turn, guide the sampling strategy of
1085 observing systems and process studies. Ensemble data assimilation systems are rapidly
1086 advancing, yielding more accurate observationally constrained ocean, atmosphere, and
1087 biogeochemical state estimates critical for sub-seasonal to decadal predictions (e.g., Penny and
1088 Hamill 2017; Verdy and Mazloff 2017). Overall, the successful coordination across observations,
1089 modeling, and theories has been critical, and these coordinated efforts will and should continue
1090 to enhance Earth system prediction skills from weather forecasts to climate projection scales.

1091

1092 *Acknowledgments*

1093 The authors of the paper are the scientists participating in the US CLIVAR Working Group on
1094 *Mesoscale and frontal-scale ocean-atmosphere interactions and influence on large-scale*
1095 *climate*. The authors thank Mike Patterson and Jennie Zhu at US CLIVAR for sponsoring the
1096 Working Group activities. We acknowledge Susan Sholi (WHOI) for her assistance in editing the
1097 final manuscript.

1098

1099 *Data Availability Statement*

1100 Datasets used in the figures are based on ERA5 (Hersbach et al. 2020), climate model
1101 simulations from the HighResMIP (Haarsma et al. 2016), or already published papers as cited in
1102 the figure captions.

1103

1104 **References**

- 1105 Alexander, M. A., and J. D. Scott, 1997: Surface flux variability over the North Pacific and
1106 North Atlantic Oceans. *J. Climate*, **10**, 2963-2978.
- 1107 Alexander, M. A., S. Shin, J. D. Scott, E. Curchitser, and C. Stock, 2020: The Response of the
1108 Northwest Atlantic Ocean to Climate Change. *J. Climate*, **33**, 405-428.
- 1109 Arduin, F., S. T. Gille, D. Menemenlis, C. B. Rocha, N. Rasche, B. Chapron, J. Gula, and J.
1110 Molemaker, 2017: Small-scale open ocean currents have large effects on wind wave
1111 heights. *J. Geophys. Res. Oceans*, **122**, 4500–4517.
- 1112 Arduin, F., and Coauthors, 2019: Observing Sea States. *Front. Mar. Sci.* **6**, 124.
- 1113 Ayet, A., N. Rasche, B. Chapron, F. Couvreur, and L. Terray, 2021: Uncovering air-sea
1114 interaction in oceanic submesoscale frontal regions using high-resolution satellite
1115 observations. *US CLIVAR Variations*, **19**, 10-17.
- 1116 Bachman, S. D., J. R. Taylor, K. A. Adams, and P. J. Hosegood, 2017: Mesoscale and
1117 Submesoscale Effects on Mixed Layer Depth in the Southern Ocean. *J. Phys. Oceanogr.*,
1118 **47**, 2173-2188.
- 1119 Bachman, S. D., B. Fox-Kemper, and F. O. Bryan, 2020: A diagnosis of anisotropic eddy
1120 diffusion from a high-resolution global ocean model. *J. Adv. Model. Earth Syst.*, **12**,
1121 e2019MS001904.
- 1122 Battisti, D., E. Sarachik, and A. Hirst, 1999: A consistent model for the large-scale steady
1123 surface atmospheric circulation in the tropics. *J. Climate*, **12**, 2956–2964.
- 1124 Beal, R. C., V. N. Kudryavtsev, D. R. Thompson, S. A. Grodsky, D. G. Tilley, V. A. Dulov, and
1125 H. C. Graber, 1997: The influence of the marine atmospheric boundary layer on ERS 1
1126 synthetic aperture radar imagery of the Gulf Stream. *J. Geophys. Res.*, **102**, 5799– 5814.
- 1127 Bellucci, A., Athanasiadis, P., Scoccimarro, E., Ruggieri, P., Gualdi, S., Fedele, R., Haarsma, R.
1128 J., Garcia-Serrano, J., Castrillo, M., Putrasahan, D., Sanchez-Gomez E., Moine, M.-
1129 P., Roberts, C. D., Roberts, M. J., Seddon, J., and Vidale, P. L., 2021: Air-Sea interaction
1130 over the Gulf Stream in an ensemble of HighResMIP present climate simulations. *Clim*
1131 *Dyn.*, **56**, 2093–2111.
- 1132 Belmonte Rivas, M., and A. Stoffelen, 2019: Characterizing ERA-interim and ERA5 surface
1133 wind biases using ASCAT. *Ocean Sci. Discuss.*, **15**, 831–852.

1134 Bilgen, S. I., and B. P. Kirtman, 2020: Impact of ocean model resolution on understanding the
 1135 delayed warming of the Southern Ocean. *Environ. Res. Lett.*, **15**, 114012.

1136 Bishop, S. P., R. J. Small, F. O. Bryan, and R. A. Tomas, 2017: Scale dependence of mid-latitude
 1137 air-sea interaction. *J. Climate*, **30**, 8207–8221.

1138 Bishop, S. P., R. J. Small, and F. O. Bryan, 2020: The global sink of available potential energy
 1139 by mesoscale air-sea interaction. *J. Adv. Model. Earth Syst.*, **12**, e2020MS002118.

1140 Bladé, I., 1997: The Influence of Midlatitude Ocean-Atmosphere Coupling on the Low-
 1141 Frequency Variability of a GCM. Part I: No Tropical SST Forcing. *J. Climate*, **10**, 2087-
 1142 2106.

1143 Bony, S., Stevens, B., Ament, F. et al., 2017: EUREC4A: A Field Campaign to Elucidate the
 1144 Couplings Between Clouds, Convection and Circulation. *Surv. Geophys.*, **38**, 1529–1568.

1145 Bourassa, M. A., and Coauthors, 2013: High-latitude ocean and sea ice surface fluxes:
 1146 requirements and challenges for climate research. *Bull. Amer. Meteo. Soc.*, **94**, 403–423.

1147 Bourassa, M. A., E. Rodríguez, and D. B. Chelton, 2016: Winds and Currents Mission: Ability to
 1148 observe mesoscale AIR/SEA coupling. *Geosci. and Remote Sens. Symposium (IGARSS)*,
 1149 [doi: 10.1109/IGARSS.2016.7730928](https://doi.org/10.1109/IGARSS.2016.7730928).

1150 Bourassa, M. A., and Coauthors 2019: Remotely Sensed Winds and Wind Stresses for Marine
 1151 Forecasting and Ocean Modeling. *Front. Mar. Sci.*, **6**, 443.

1152 Booth, J. F., L. Thompson, J. Patoux, K. A. Kelly, and S. Dickinson, 2010: The signature of
 1153 midlatitude tropospheric storm tracks in the surface winds. *J. Climate*, **23**, 1160–1174.

1154 Booth, J. F., L. Thompson, J. Patoux, and K. A. Kelly, 2012: Sensitivity of midlatitude
 1155 storm intensification to perturbations in the sea surface temperature near the Gulf Stream.
 1156 *Mon. Wea. Rev.*, **140**, 1241–1256.

1157 Booth, J. F., Y. O. Kwon, S. Ko, R. J. Small, and R. Msadek, 2017: Spatial patterns and intensity
 1158 of the surface storm tracks in CMIP5 models. *J. Climate*, **30**, 4965–4981.

1159 Brachet, S., F. Codron, Y. Feliks, M. Ghil, H. Le Treut, and E. Simonnet, 2012:
 1160 Atmospheric Circulations Induced by a Midlatitude SST Front: A GCM Study. *J.*
 1161 *Climate*, **25**, 1847–1853.

1162 Brankart, J.-M., 2013: Impact of uncertainties in the horizontal density gradient upon low
 1163 resolution global ocean modelling. *Ocean Modell.*, **66**, 64-76.

1164 Bryan, F. O., R. Tomas, J. M. Dennis, D. B. Chelton, N. G. Loeb, and J. L. McClean, 2010:
1165 Frontal Scale Air-Sea Interaction in High-Resolution Coupled Climate Models. *J.*
1166 *Climate*, **23**, 6277-6291.

1167 Bye, J. A. T., 1986: Momentum exchange at the sea surface by wind stress and understress.
1168 *Quart. J. Roy. Met. Soc.*, **112**, 501–510.

1169 Cavaleri, L., B. Fox-Kemper, and M. Hemer, 2012: Wind waves in the coupled climate
1170 system. *Bull. Amer. Meteorol. Soc.*, **93**, 1651–1661.

1171 Centurioni, L. R. and Coauthors, 2019: Global in situ Observations of Essential Climate and
1172 Ocean Variables at the Air-Sea Interface. *Front. Mar. Sci.*, **6**, 419.

1173 Chang, E. K. M., S. Lee, and K. L. Swanson, 2002. Storm Track Dynamics. *J. Climate*, **15**,
1174 2163-2183.

1175 Chang, P., and Coauthors, 2020: An unprecedented set of high-resolution Earth system
1176 simulations for understanding multiscale interactions in climate variability and change. *J.*
1177 *Adv. Model. Earth Sys.* **12**, e2020MS002298.

1178 Charney, J. G., 1947: The dynamics of long waves in a baroclinic westerly current. *J.*
1179 *Meteor.*, **4**, 135–162.

1180 Chelton, D. B., and Coauthors, 2001: Observations of coupling between surface wind stress and
1181 sea surface temperature in the eastern tropical Pacific. *J. Climate*, **14**, 1479–1498.

1182 Chelton, D. B., M. G. Schlax, M. H. Freilich, and R. F. Milliff, 2004: Satellite measurements
1183 reveal persistent small-scale features in ocean winds. *Science*, **303**, 978–983.

1184 Chelton, D. B., 2005: The Impact of SST Specification on ECMWF Surface Wind Stress Fields
1185 in the Eastern Tropical Pacific. *J. Climate*, **18**, 530-550.

1186 Chelton, D. B., M. G. Schlax and R. M. Samelson, 2007: Summertime Coupling between Sea
1187 Surface Temperature and Wind Stress in the California Current System. *J. Phys.*
1188 *Oceanogr.*, **37**, 495-517.

1189 Chelton, D. B., and S.-P. Xie, 2010: Coupled ocean-atmosphere interaction at oceanic
1190 mesoscales. *Oceanogr.*, **23**, 52-69.

1191 Chelton, D. B., P. Gaube, M. G. Schlax, J. J. Early, and R. M. Samelson, 2011a: The Influence
1192 of Nonlinear Mesoscale Eddies on Near-Surface Oceanic Chlorophyll. *Science*, **334**,
1193 328–332.

1194 Chelton, D. B., M. G. Schlax, and R. M. Samelson, 2011b: Global observations of nonlinear
1195 mesoscale eddies. *Prog. Oceanogr.*, **91**, 167-216.

1196 Clayson, C. A., J. B. Edson, A. Paget, R. Graham, and B. Greenwood, 2019: The effects of
1197 rainfall on the atmosphere and the ocean during SPURS-2. *Oceanogr.*, **32**, 86–97.

1198 Cravatte, S., W. S. Kessler, N. Smith, S. E. Wijffels, and Contributing Authors, 2016: First
1199 Report of TPOS 2020. GOOS-215, 200 pp. [Available online at [http://tpos2020.org/first-](http://tpos2020.org/first-report/)
1200 [report/.](http://tpos2020.org/first-report/)]

1201 Cronin, M. F., S.-P. Xie, and H. Hashizume, 2003: Barometric pressure variations associated
1202 with eastern Pacific tropical instability waves. *J. Climate*, **16**, 3050- 3057.

1203 Cronin, M. F., S. Legg, and P. Zuidema, 2009: Best practices for process studies. *Bull. Amer.*
1204 *Meteor. Soc.*, **90**, 917–918.

1205 Cronin, M. F., and Coauthors, 2019: Air-Sea Fluxes with a Focus on Heat and Momentum.
1206 *Front. Mar. Sci.*, **6**, 430.

1207 Czaja, A., and N. Blunt, 2011: A new mechanism for ocean-atmosphere coupling in
1208 midlatitudes. *Quart. J. Roy. Met. Soc.*, **137**, 1095–1101.

1209 Czaja, A., C. Frankignoul, S. Minobe, and B. Vanni re, 2019: Simulating the Midlatitude
1210 Atmospheric Circulation: What Might We Gain From High-Resolution Modeling of Air-
1211 Sea Interactions? *Curr. Clim. Change Rep.*, **5**, 390–406.

1212 Dacre, H. F., and S. L. Gray, 2013: Quantifying the climatological relationship between
1213 extratropical cyclone intensity and atmospheric precursors. *Geophys. Res.*
1214 *Lett.*, **40**, 2322– 2327.

1215 D’Asaro, E., C. Lee, L. Rainville, R. Harcourt, and L. Thomas, 2011: Enhanced Turbulence and
1216 Energy Dissipation at Ocean Fronts. *Science*, **332**, 318-322.

1217 D’Asaro, E., and Coauthors, 2018: Ocean convergence and dispersion of flotsam. *Proc. Natl.*
1218 *Acad. Sci.*, **115**, 1162–1167.

1219 Davis, C. A., and K. A. Emanuel, 1988: Observational Evidence for the Influence of Surface
1220 Heat Fluxes on Rapid Maritime Cyclogenesis. *Mon. Wea. Rev.*, **116**, 2649-2659.

1221 de Boyer Mont gut, C., G. Madec, A. S. Fischer, A. Lazar, and D. Iudicone, 2004: Mixed layer
1222 depth over the global ocean: An examination of profile data and a profile-based
1223 climatology. *J. Geophys. Res.*, **109**, C12003.

- 1224 de Kloe, J., A. Stoffelen, and A. Verhoef, 2017: Improved use of scatterometer measurements by
1225 using stress-equivalent reference winds. *IEEE J. Sel. Top. Appl. Earth Observ. Remote*
1226 *Sens.*, **10**, 2340–2347.
- 1227 de Szoeke, S. P., and C. S. Bretherton, 2004: Quasi-Lagrangian large eddy simulations of cross-
1228 equatorial flow in the east Pacific atmospheric boundary layer. *J. Atmos. Sci.*, **61**, 1837-
1229 1858.
- 1230 de Szoeke, S. P., and E. D. Maloney, 2020: Atmospheric Mixed Layer Convergence from
1231 Observed MJO Sea Surface Temperature Anomalies. *J. Climate*, **33**, 547-558.
- 1232 de Szoeke, S. P., J. B. Edson, J. R. Marion, C. W. Fairall, and L. Bariteau, 2015: The MJO and
1233 Air–Sea Interaction in TOGA COARE and DYNAMO. *J. Climate*, **28**, 597–622.
- 1234 Deike, L., and W. K. Melville, 2018: Gas transfer by breaking waves. *Geophys. Res. Lett.*, **45**,
1235 10,482–10,492.
- 1236 Deser, C., R. A. Tomas, and S. Peng, 2007: The Transient Atmospheric Circulation Response to
1237 North Atlantic SST and Sea Ice Anomalies. *J. Climate*, **20**, 4751-4767.
- 1238 Deskos, G., J. C. Y. Lee, C. Draxl, and M. A. Sprague, 2021: Review of wind-wave coupling
1239 models for large-eddy simulation of the marine atmospheric boundary layer. *J. Atmos.*
1240 *Sci.*, **78**, 3025-3045
- 1241 Dewar, W., and G. Flierl, 1987: Some effects of the wind on rings. *J. Phys. Oceanogr.*, **17**,
1242 1653–1667.
- 1243 Dong, J., B. Fox-Kemper, H. Zhang, and C. Dong, 2020: The scale of submesoscale baroclinic
1244 instability globally. *J. Phys. Oceanogr.*, **50**, 2649–2667.
- 1245 Dong, J., B. Fox-Kemper, H. Zhang, and C. Dong, 2021: The Scale and Activity of Symmetric
1246 Instability Estimated from a Global Submesoscale-Permitting Ocean Model. *J. Phys.*
1247 *Oceanogr.*, **51**, 1655-1670.
- 1248 Doyle, J. D., and Coauthors, 2017: A view of tropical cyclones from above: The Tropical
1249 Cyclone Intensity Experiment. *Bull. Amer. Meteor. Soc.*, **98**, 2113–2134.
- 1250 Drivas, T. D., D. D. Holm, and J. M. Leahy, 2020: Lagrangian Averaged Stochastic Advection
1251 by Lie Transport for Fluids. *J. Stat. Phys.*, **179**, 1304–1342.
- 1252 du Plessis, M., S. Swart, I. J. Ansorge, A. Mahadevan, and A. F. Thompson, 2019: Southern
1253 Ocean Seasonal Restratification Delayed by Submesoscale Wind–Front Interactions. *J.*
1254 *Phys. Oceanogr.*, **49**, 1035-1053.

1255 Dufois, F., N. J. Hardman-Mountford, M. Fernandes, B. Wojtasiewicz, D. Shenoy, D. Slawinski,
1256 M. Gauns, J. Greenwood, and R. Toresen, 2017: Observational insights into chlorophyll
1257 distributions of subtropical South Indian Ocean eddies. *Geophys. Res. Lett.*, **44**, 3255–
1258 3264.

1259 Eady, E., 1949: Long waves and cyclone waves. *Tellus*, **1**, 33–52.

1260 Edson, J. B., and C. W. Fairall, 1998: Similarity relationships in the marine atmospheric surface
1261 layer for terms in the TKE and scalar variance budgets. *J. Atmos. Sci.*, **55**, 2311–2328.

1262 Edson, J. B., C. W. Fairall, L. Bariteau, C. J. Zappa, A. Cifuentes-Lorenzen, W. M. McGillis, S.
1263 Pezoa, J. E. Hare, and D. Helmig, 2011: Direct-covariance measurement of CO₂ gas
1264 transfer velocity during the 2008 Southern Ocean Gas Exchange Experiment. *J. Geophys.*
1265 *Res.*, **116**, C00F10.

1266 Edson, J. B., V. Jampana, R. Weller, S. Bigorre, A. Plueddemann, C. Fairall, S. Miller, L.
1267 Mahrt, D. Vickers, and H. Hersbach, 2013: On the exchange of momentum over the open
1268 ocean. *J. Phys. Oceanogr.*, **43**, 1589–1610.

1269 Fairall C. W., E. F. Bradley, D. P. Rogers, J. D. Edson, and G. S. Young, 1996: Bulk
1270 parameterization of air-sea fluxes for Tropical Ocean Global Atmosphere Coupled-Ocean
1271 Atmosphere Response Experiment. *J. Geophys. Res.*, **15**, 3747-3764.

1272 Fairall, C.W., E.F. Bradley, J.E. Hare, A.A. Grachev, and J.B. Edson, 2003: Bulk
1273 parameterization of air-sea fluxes: Updates and verification for the COARE algorithm. *J.*
1274 *Climate*, **16**, 571-591.

1275 Fairall, C. W., M. Yang, L. Bariteau, J. B. Edson, D. Helmig, W. McGillis, S. Pezoa, J. E. Hare,
1276 B. Huebert, and B. Blomquist, 2011: Implementation of the COARE algorithm with O₃,
1277 CO₂ and DMS. *J. Geophys. Res.*, **116**, C00F09.

1278 Farrar, J. T., and Coauthors, 2020: S-MODE: The Sub-Mesoscale Ocean Dynamics Experiment.
1279 *IGARSS 2020-2020 IEEE International Geoscience and Remote Sensing Symposium.*
1280 3533-3536. 10.1109/IGARSS39084.2020.9323112.

1281 Feliks, Y., M. Ghil, and E. Simonnet, 2004: Low-frequency variability in the midlatitude
1282 atmosphere induced by an oceanic thermal front. *J. Atmos. Sci.*, **61**, 961–981.

1283 Ferreira, D., and C. Frankignoul, 2005: The transient atmospheric response to midlatitude SST
1284 anomalies. *J. Climate*, **18**, 1049-1067.

1285 Ferreira, D., and C. Frankignoul, 2008: Transient atmospheric response to interactive SST
1286 anomalies. *J. Climate*, **21**, 584-592.

1287 Fox-Kemper, B., R. Ferrari, and R. Hallberg, 2008: Parameterization of mixed layer eddies. I:
1288 Theory and diagnosis. *J. Phys. Oceanogr.*, **38**, 1145-1165.

1289 Fox-Kemper, B., G. Danabasoglu, R. Ferrari, S. M. Griffies, R. W. Hallberg, M. M. Holland, M.
1290 E. Maltrud, S. Peacock, and B. L. Samuels, 2011: Parameterization of mixed layer
1291 eddies. III: Implementation and impact in global ocean climate simulations. *Ocean*
1292 *Modell.*, **39**, 61-78.

1293 Fox-Kemper, B., S. Marsland, E. Chassignet, E. Curchitser, S. Griffies, I. Montes, H. Seo, A. M.
1294 Treguier, and W. Weijer, 2019: Sources and sinks of ocean mesoscale eddy energy. 5,
1295 page 21. A Joint US CLIVAR and CLIVAR Workshop Report. Available from
1296 <http://dx.doi.org/10.5065/CH5R-5034>.

1297 Foussard, A., G. Lapeyre, and R. Plougonven, 2019a: Response of surface wind divergence to
1298 mesoscale SST anomalies under different wind conditions. *J. Atmos. Sci.*, **76**, 2065-2082.

1299 Foussard, A., G. Lapeyre, and R. Plougonven, 2019b: Storm Track Response to Oceanic Eddies
1300 in Idealized Atmospheric Simulations. *J. Climate*, **32**, 445-463.

1301 Frankignoul, C., 1985: Sea surface temperature anomalies, planetary waves, and air-sea feedback
1302 in midlatitudes. *Rev. Geophys.*, **23**, 357-390.

1303 Frankignoul, C., and K. Hasselmann, 1977; Stochastic climate models, Part II Application to sea-
1304 surface temperature anomalies and thermocline variability. *Tellus*, **29**, 289-305.

1305 Frankignoul, C., N. Sennechael, Y.-O. Kwon, and M. A. Alexander, 2011: Influence of the
1306 meridional shifts of the Kuroshio and the Oyashio Extensions on the atmospheric
1307 circulation. *J. Climate*, **24**, 762-777.

1308 Frenger, I., N. Gruber, R. Knutti, and M. Münnich, 2013: Imprint of Southern Ocean eddies on
1309 winds, clouds and rainfall. *Nature Geosci.*, **6**, 608-612.

1310 Frew, N. M., D. M. Glover, E. J. Bock, and S. J. McCue, 2007: A new approach to estimation of
1311 global air-sea gas transfer velocity fields using dual-frequency altimeter backscatter. *J.*
1312 *Geophys. Res.*, **112**, C11003.

1313 Friehe, C. A., W. J. Shaw, D. P. Rogers, K. L. Davidson, W. G. Large, S. A. Stage, G. H.
1314 Crescenti, S. J. S. Khalsa, G. K. Greenhut, and F. Li, 1991: Air-sea fluxes and surface
1315 layer turbulence around a sea surface temperature front, *J. Geophys. Res.*, **96**, 8593-8609.

1316 Gade, M., and A. Stoffelen, 2019: An Introduction to Microwave Remote Sensing of the Asian
1317 Seas. In: Barale V., Gade M. (eds) Remote Sensing of the Asian Seas. Springer,
1318 Cham. https://doi.org/10.1007/978-3-319-94067-0_4.

1319 Gaube, P., D. B. Chelton, P. G. Strutton, and M. J. Behrenfeld, 2013: Satellite observations of
1320 chlorophyll, phytoplankton biomass, and Ekman pumping in nonlinear mesoscale eddies.
1321 *J. Geophys. Res. Oceans*, **118**, 6349–6370.

1322 Gaube, P., D. J. McGillicuddy, D. B. Chelton, M. J. Behrenfeld, and P. G. Strutton, 2014:
1323 Regional variations in the influence of mesoscale eddies on near-surface chlorophyll. *J.*
1324 *Geophys. Res. Oceans*, **119**, 8195-8220.

1325 Gaube, P. D. B. Chelton, R. M. Samelson, M. G. Schlax, and L. W. O’Neill, 2015: Satellite
1326 Observations of Mesoscale Eddy-Induced Ekman Pumping. *J. Phys. Oceanogr.*, **45**, 104–
1327 132.

1328 Gaube, P., C. C. Chickadel, R. Branch, and A. Jessup, 2019: Satellite observations of SST-
1329 induced wind speed perturbation at the oceanic submesoscale. *Geophys. Res. Lett.*, **46**,
1330 2690–2695.

1331 Gent, P. R., and J. C. McWilliams, 1990: Isopycnal Mixing in Ocean Circulation Models. *J.*
1332 *Phys. Oceanogr.*, **20**, 150-155.

1333 Gentemann, C., C. A. Clayson, S. Brown, T. Lee, R. Parfitt, J. T. Farrar, M. Bourassa, P. J.
1334 Minnett, H. Seo, S. T. Gille, and V. Zlotnicki, 2020: FluxSat: Measuring the ocean-
1335 atmosphere turbulent exchange of heat and moisture from space. *Remote Sens.*, **12**, 1796.

1336 Gervais, M., J. Shaman, and Y. Kushnir, 2018: Mechanisms Governing the Development of the
1337 North Atlantic Warming Hole in the CESM-LE Future Climate Simulations. *J.*
1338 *Climate*, **31**, 5927-5946.

1339 Graber, H. C., E. A. Terray, M. A. Donelan, W. M. Drennan, J. C. Van Leer, and D. B. Peters,
1340 2000: ASIS—A New Air–Sea Interaction Spar Buoy: Design and Performance at Sea. *J.*
1341 *Atmos. Ocean Tech.*, **17**, 708-720.

1342 Gommenginger, C., and Coauthors, 2019: SEASTAR: A Mission to Study Ocean Submesoscale
1343 Dynamics and Small-Scale Atmosphere-Ocean Processes in Coastal, Shelf and Polar
1344 Seas. *Front. Mar. Sci.*, **6**, 457.

1345 Grist, J. P., S. A. Josey, B. Sinha, J. L. Catto, M. J. Roberts, and A. C. Coward, 2021: Future
1346 evolution of an eddy rich ocean associated with enhanced east Atlantic storminess in a
1347 coupled model projection. *Geophys. Res. Lett.*, **48**, e2021GL092719.

1348 Haarsma, R. J., M. Roberts and Coauthors, 2016: High Resolution Model
1349 Intercomparison Project (HighResMIP). *Geosci Model Dev.*, **9**, 4185–4208.

1350 Hallberg, R., 2013: Using a resolution function to regulate parameterizations of oceanic
1351 mesoscale eddy effects. *Ocean Modell.*, **72**, 92-103.

1352 Hand, R., and Coauthors, 2014: Simulated response to inter-annual SST variations in the Gulf
1353 Stream region. *Clim Dyn* **42**, 715–731.

1354 Haney, S., B. Fox-Kemper, K. Julien, and A. Webb, 2015: Symmetric and geostrophic
1355 instabilities in the wave-forced ocean mixed layer. *J. Phys. Oceanogr.*, **45**, 3033–3056.

1356 Harrison, C. S., M. C. Long, N. S. Lovenduski, and J. K. Moore, 2018: Mesoscale effects on
1357 carbon export: a global perspective. *Glob. Biogeochem. Cycles*, **32**, 680–703.

1358 Hashizume, H., S.-P. Xie, M. Fujiwara, M. Shiotani, T. Watanabe, Y. Tanimoto, W. T. Liu, and
1359 K. Takeuchi, 2002: Direct observations of atmospheric boundary layer response to SST
1360 variations associated with tropical instability waves over the eastern equatorial Pacific. *J.*
1361 *Climate*, **15**, 3379–3393.

1362 Hausmann, U., D. J. McGillicuddy, and J. Marshall, 2017: Observed mesoscale eddy signatures
1363 in Southern Ocean surface mixed-layer depth. *J. Geophys. Res. Oceans*, **122**, 617–635,

1364 Hawcroft, M. K., L. C. Shaffrey, K. I. Hodges, and H. F. Dacre, 2012: How much Northern
1365 Hemisphere precipitation is associated with extratropical cyclones? *Geophys. Res.*
1366 *Lett.*, **39**, L24809.

1367 Hayasaki, M., R. Kawamura, M. Mori, and M. Watanabe, 2013: Response of extratropical
1368 cyclone activity to the Kuroshio large meander in northern winter. *Geophys. Res.*
1369 *Lett.*, **40**, 2851–2855.

1370 Hayes, S. P., M. J. McPhaden, and J. M. Wallace, 1989: The Influence of Sea Surface
1371 Temperature on Surface Wind in the Eastern Equatorial Pacific: Weekly to Monthly
1372 Variability. *J. Climate*, **2**, 1500-1506.

1373 Hersbach, H., and Coauthors, 2020: The ERA5 global reanalysis. *Quart. J. Roy. Met. Soc.*, **146**,
1374 1999-2049.

1375 Hirata, H., R. Kawamura, M. Nonaka, and K. Tsuboki, 2019: Significant impact of heat supply
1376 from the Gulf Stream on a “superbomb” cyclone in January 2018. *Geophys. Res.*
1377 *Lett*, **46**, 7718–7725.

1378 Hirata, H., and M. Nonaka, 2021: Impacts of strong warm ocean currents on development of
1379 extratropical cyclones through the warm and cold conveyor belts: A review. Elsevier,
1380 9780128181577, 267-293 pp., [doi:http://www.sciencedirect.com/science/article/pii/B9780128181560000149](https://doi.org/10.1016/B9780128181560000149).

1382 Hogg, A., W. K. Dewar, P. Berloff, S. Kravtsov, and D. K. Hutchinson, 2009: The effects of
1383 mesoscale ocean-atmosphere coupling on the large-scale ocean circulation. *J.*
1384 *Climate*, **22**, 4066-4082.

1385 Holton, J. R., 1965a: The influence of viscous boundary layers on transient motions in a
1386 stratified rotating fluid. Part I. *J. Atmos. Sci.*, **22**, 402–411.

1387 Holton, J. R., 1965b: The influence of viscous boundary layers on transient motions in a
1388 stratified rotating fluid. Part II. *J. Atmos. Sci.*, **22**, 535– 540.

1389 Hoskins, B. J., and D. J. Karoly, 1981: The steady linear response of a spherical atmosphere to
1390 thermal and orographic forcing, *J. Atmos. Sci.*, **38**, 1179-1196.

1391 Hoskins, B. J., and K. I. Hodges, 2002: New Perspectives on the Northern Hemisphere Winter
1392 Storm Tracks. *J. Atmos. Sci.*, **59**, 1041–1061.

1393 Hoskins, B. J., and P. J. Valdes, 1990: On the existence of storm tracks. *J. Atmos. Sci.*, **47**, 1854–
1394 1864.

1395 Hotta, D., and H. Nakamura, 2011: On the significance of sensible heat supply from the ocean in
1396 the maintenance of mean baroclinicity along storm tracks. *J. Climate*, **24**, 3377–3401.

1397 Infanti, J. M., and B. P. Kirtman, 2019: A comparison of CCSM4 high-resolution and low-
1398 resolution predictions for south Florida and southeast United States drought. *Clim.*
1399 *Dynm.*, **52**, 6877-6892.

1400 IPCC, 2021: Climate Change 2021. The Physical Science Basis. Contribution of Working Group
1401 I to the Sixth Assessment Report of the Intergovernmental Panel on Climate Change
1402 [Masson-Delmotte, V., P. Zhai, A. Pirani, S.L. Connors, C. Péan, S. Berger, N. Caud, Y.
1403 Chen, L. Goldfarb, M.I. Gomis, M. Huang, K. Leitzell, E. Lonnoy, J.B.R. Matthews,
1404 T.K. Maycock, T. Waterfield, O. Yelekçi, R. Yu, and B. Zhou (eds.)]. Cambridge
1405 University Press. In Press.

1406 Jackson, L. C., and Coauthors, 2020: Impact of ocean resolution and mean state on the rate of
1407 AMOC weakening. *Clim. Dyn.*, **55**, 1711–1732.

1408 Jansen, M. F., and I. M. Held, 2014: Parameterizing subgrid-scale eddy effects using
1409 energetically consistent backscatter. *Ocean Modell.*, **80**, 36–48.

1410 Johnson, L., C. M. Lee, and E. A. D’Asaro, 2016: Global Estimates of Lateral Springtime
1411 Restratification. *J. Phys. Oceanogr.*, **46**, 1555–1573.

1412 Jones, D. G., and Coauthors, 2015: Developments since 2005 in understanding potential
1413 environmental impacts of CO₂ leakage from geological storage. *Int. J. Greenh. G.*
1414 *Con.*, **40**, 350–377.

1415 Jullien, S., S. Masson, V. Oerder, G. Samson, F. Colas, and L. Renault, 2020: Impact of ocean-
1416 atmosphere current feedback on the ocean mesoscale activity: regional variations, and
1417 sensitivity to model resolution. *J. Climate*, **33**, 2585–2602.

1418 Jury, M. R., and S. Courtney, 1991: A transition in weather over the Agulhas Current. *S. Afr. J.*
1419 *Mar. Sci.*, **10**, 159–171.

1420 Karmalkar, A.V., and R. M. Horton, 2021: Drivers of exceptional coastal warming in the
1421 northeastern United States. *Nat. Clim. Chang.*, **11**, 854–860.

1422 Kaspi, Y., and T. Schneider, 2013: The role of stationary eddies in shaping midlatitude storm
1423 tracks. *J. Atmos. Sci.*, **70**, 2596–2613.

1424 Keil, P., and Coauthors, 2020: Multiple drivers of the North Atlantic warming hole. *Nat. Clim.*
1425 *Chang.*, **10**, 667–671.

1426 Kelly, K. A., S. Dickinson, M. J. McPhaden, and G. C. Johnson, 2001: Ocean Currents Evident
1427 in Satellite Wind Data. *Geophys. Res. Lett.*, **28**, 2469–2472.

1428 Kelly, K. A., R. J. Small, R. M. Samelson, B. Qiu, T. M. Joyce, Y. Kwon, and M. F. Cronin,
1429 2010: Western Boundary Currents and Frontal Air–Sea Interaction: Gulf Stream and
1430 Kuroshio Extension. *J. Climate*, **23**, 5644–5667.

1431 Kessler, W.S., S. E. Wijffels, S. Cravatte, N. Smith, and Contributing Authors, 2019: Second
1432 Report of TPOS 2020. GOOS-234, 265 pp. [Available online
1433 at <http://tpos2020.org/second-report/>].

1434 Kilpatrick, T., N. Schneider, and B. Qiu, 2014: Boundary layer convergence induced by strong
1435 winds across a midlatitude SST front. *J. Climate*, **27**, 1698–1718.

1436 Kilpatrick, T., N. Schneider, and B. Qiu, 2016: Atmospheric response to a midlatitude SST front:
1437 Alongfront winds. *J. Atmos. Sci.*, **73**, 3489–3509.

1438 Kirincich, A., B. Emery, L. Washburn, and P. Flament, 2019: Improving Surface Current
1439 Resolution Using Direction Finding Algorithms for Multiantenna High-Frequency
1440 Radars, *J. Atmos. and Oceanic Technol.*, **36**, 1997-2014.

1441 Kirtman, B. P., and Coauthors, 2012: Impact of ocean model resolution on CCSM climate
1442 simulations. *Clim. Dyn.*, **39**, 1303– 1328.

1443 Kudryavtsev, V., B. Chapron, and V. Makin, 2014: Impact of wind waves on the air-sea fluxes:
1444 A coupled model. *J. Geophys. Res. Oceans*, **119**, 1217-1236.

1445 Kushnir, Y., W. A. Robinson, I. Blade, N. M. J. Hall, S. Peng, and R. Sutton, 2002: Atmospheric
1446 GCM response to extratropical SST anomalies: Synthesis and evaluation. *J. Climate*, **15**,
1447 2233-2256.

1448 Kuwano-Yoshida, A., and S. Minobe, 2017. Storm track response to SST fronts in the
1449 Northwestern Pacific region in an AGCM. *J. Climate*, **30**, 1081-1102.

1450 Kwak, K. H. Song, J. Marshall, H. Seo, and D. McGillicuddy, Jr., 2021: Suppressed pCO₂ in the
1451 Southern Ocean due to the interaction between current and wind. *J. Geophys. Res.*
1452 *Oceans*, <https://doi.org/10.1029/2021JC017884>.

1453 Kwon, Y.-O., M. A. Alexander, N. A. Bond, C. Frankignoul, H. Nakamura, B. Qiu, and L. A.
1454 Thompson, 2010. Role of the Gulf Stream and Kuroshio-Oyashio Systems in Large-Scale
1455 Atmosphere-Ocean Interaction: A Review. *J. Climate*, **23**, 3249-3281.

1456 Kwon, Y.-O., and T. M. Joyce, 2013: Northern Hemisphere Winter Atmospheric Transient Eddy
1457 Heat Fluxes and the Gulf Stream and Kuroshio-Oyashio Extension Variability. *J.*
1458 *Climate*, **26**, 9839-9859.

1459 Lambaerts, J., G. Lapeyre, R. Plougonven, and P. Klein, 2013: Atmospheric response to sea
1460 surface temperature mesoscale structures. *J. Geophys. Res. Atmos.*, **118**, 9611–9621.

1461 Lac, C., and Coauthors, 2018: Overview of the Meso-NH model version 5.4 and its applications.
1462 *Geosci. Model Dev.*, **11**, 1929-1969.

1463 Lane, E. M., J. M. Restrepo, and J. C. McWilliams, 2007: Wave–current interaction: A
1464 comparison of radiation-stress and vortex-force representations. *J. Phys. Oceanogr.*,
1465 **37**, 1122–1141.

1466 Laurindo, L. C., A. Mariano, and R. Lumpkin, 2017: An improved surface velocity climatology
1467 for the global ocean from drifter observations. *Deep Sea Res. I*, **124**, 73–92.

1468 Laurindo, L. C., L. Siqueira, A. J. Mariano, and B. Kirtman, 2019: Cross-spectral analysis of the
1469 SST/10-m wind speed coupling resolved by satellite products and climate model
1470 simulations. *Clim. Dyn.*, **52**, 5071–5098.

1471 Lee, R. W., T. J. Woollings, B. J. Hoskins, K. D. Williams, C. H. O’Reilly, and G. Masato, 2018:
1472 Impact of Gulf Stream SST biases on the global atmospheric circulation. *Clim Dyn.*, **51**,
1473 3369–3387.

1474 Leibovich, S., 1983: The Form and Dynamics of Langmuir Circulations. *Annu. Rev. Fluid*
1475 *Mech.*, **15**, 391-427.

1476 Lenschow, D. H., P. B. Krummel, and S. T. Siems, 1999: Measuring Entrainment, Divergence,
1477 and Vorticity on the Mesoscale from Aircraft. *J. Atmos. Ocean Tech.*, **16**, 1384-1400.

1478 Lévy, M., 2008: The modulation of biological production by oceanic mesoscale turbulence. In
1479 *Transport and Mixing in Geophysical Flows*, ed. J Weiss, A Provenzale, pp. 219–61.
1480 Berlin: Springer

1481 Lévy, M., P. J. S. Franks, and K. S. Smith, 2018: The role of submesoscale currents in
1482 structuring marine ecosystems. *Nat. Commun.*, **9**, 4758.

1483 Li, Y., and R. E. Carbone, 2012: Excitation of rainfall over the tropical western Pacific. *J. Atmos.*
1484 *Sci.*, **69**, 2983–2994.

1485 Lindzen, R. S., and B. Farrell, 1980: A Simple Approximate Result for the Maximum Growth
1486 Rate of Baroclinic Instabilities. *J. Atmos. Sci.*, **37**, 1648-1654.

1487 Lindzen, R. S., and S. Nigam, 1987: On the role of sea surface temperature gradients in forcing
1488 low-level winds and convergence in the tropics. *J. Atmos. Sci.*, **44**, 2418–2436.

1489 Liu, W., A. V. Fedorov, S.-P. Xie, and S. Hu, 2020: Climate impacts of a weakened Atlantic
1490 meridional overturning circulation in a warming climate. *Science Advances*, **6**, eaaz4876.

1491 Liu, X., X. Ma, P. Chang, Y. Jia, D. Fu, G. Xu, L. Wu, R. Saravanan, and C. M. Patricola,
1492 2021: Ocean fronts and eddies force atmospheric rivers and heavy precipitation
1493 in western North America. *Nat. Commun.*, **12**, 1268.

1494 López-Dekker, P., H. Rott, P. Prats-Iraola, B. Chapron, K. Scipal, and E. D. Witte, 2019:
1495 Harmony: an Earth Explorer 10 Mission Candidate to Observe Land, Ice, and Ocean

1496 Surface Dynamics, in: IGARSS 2019 - 2019 IEEE International Geoscience and Remote
1497 Sensing Symposium, pp. 8381–8384, <https://doi.org/10.1109/IGARSS.2019.8897983>.

1498 Lorenz, E., 1960: Generation of available potential energy and the intensity of the general
1499 circulation. In R. L. Pfeffer (Ed.), Dynamics of climate (pp. 86–92). Oxford: Pergamon
1500 Press.

1501 Luo, J.-J., S. Masson, E. Roeckner, G. Madec, and T. Yamagata, 2005: Reducing Climatology
1502 Bias in an Ocean-Atmosphere CGCM with Improved Coupling Physics. *J. Climate*, **18**,
1503 2344-2360

1504 Ma, X., P. Chang, R. Saravanan, R. M. J.-S. Hsieh, D. Wu, X. Lin, L. Wu, and Z. Jing, 2015:
1505 Distant influence of Kuroshio eddies on North Pacific weather patterns. *Sci. Rep.*, **5**,
1506 17785.

1507 Ma, X., and Coauthors, 2016: Western boundary currents regulated by interaction between ocean
1508 eddies and the atmosphere. *Nature*, **535**, 533–537.

1509 Ma, X., P. Chang, R. Saravanan, R. Montuoro, H. Nakamura, D. Wu, X. Lin, and L. Wu, 2017:
1510 Importance of resolving Kuroshio Front and eddy influence in simulating the North
1511 Pacific storm track. *J. Climate*, **30**, 1861-1880.

1512 Mahrt, L., D. Vickers, and E. Moore, 2004: Flow Adjustments Across Sea-Surface Temperature
1513 Changes. *Boundary-Layer Meteorology* **111**, 553–564.

1514 Marshall, J., and Coauthors, 2009: The Climode Field Campaign: Observing the Cycle of
1515 Convection and Restratification over the Gulf Stream. *Bull. Amer. Meteor. Soc.*, **90**,
1516 1337–1350.

1517 Marshall, J., J. Scott, K. Armour, J.-M. Campin, M. Kelley, and A. Romanou, 2014: The ocean's
1518 role in the transient response of climate to abrupt greenhouse gas forcing. *Clim. Dyn.*,
1519 **44**, 2287–2299.

1520 Martin, A., and K. Richards, 2001: Mechanisms for vertical nutrient transport within a North
1521 Atlantic mesoscale eddy. *Deep Sea Res.–II*, **48**, 757–773.

1522 Masunaga, R., H. Nakamura, B. Taguchi and T. Miyasaka, 2020a: Processes Shaping the
1523 Frontal-Scale Time-Mean Surface Wind Convergence Patterns around the Kuroshio
1524 Extension in Winter. *J. Climate*, **33**, 3-25.

1525 Masunaga, R., H. Nakamura, B. Taguchi, and T. Miyasaka, 2020b: Processes Shaping
 1526 the Frontal-Scale Time-Mean Surface Wind Convergence Patterns around the
 1527 Gulf Stream and Agulhas Return Current in Winter. *J. Climate*, **33**, 9083–9101.
 1528 Masunaga, R. and N. Schneider, 2021: Surface wind responses to mesoscale sea surface
 1529 temperature over western boundary current regions assessed by spectral transfer
 1530 functions. *J. Atmos. Sci.*, submitted.
 1531 McGillicuddy, D. J., and Coauthors, 2007: Eddy/Wind Interactions Stimulate Extraordinary
 1532 Mid-Ocean Plankton Blooms. *Science*, **316**, 1201.
 1533 McGillicuddy, D. J., 2016: Mechanisms of physical-biological-biogeochemical interaction at the
 1534 oceanic mesoscale. *Ann. Rev. Mar. Sci.*, **8**, 125-159.
 1535 McGillis, W. R., J. B. Edson, J. E. Hare, and C. W. Fairall, 2001: Direct covariance air-sea CO₂
 1536 fluxes. *J. Geophys. Res.*, **106**, 16729-16745.
 1537 McLandress, C., T. Shepherd, J. Scinocca, D. Plummer, M. Sigmond, A. Jonsson, and M.
 1538 Reader, 2011: Separating the dynamical effects of climate change and ozone depletion.
 1539 Part II: Southern hemisphere troposphere. *J. Climate*, **24**, 1850–1868.
 1540 McWilliams, J. C., E. Huckle, J. Liang, and P. P. Sullivan, 2012: The Wavy Ekman Layer:
 1541 Langmuir Circulations, Breaking Waves, and Reynolds Stress. *J. Phys. Oceanogr.*, **42**,
 1542 1793-1816.
 1543 McWilliams, J. C., and B. Fox-Kemper, 2013: Oceanic wave-balanced surface fronts and
 1544 filaments. *J. Fluid Mech.*, **730**, 464-490.
 1545 Meinig, C., and Coauthors, 2019: Public-Private Partnerships to Advance Regional Ocean-
 1546 Observing Capabilities: A Saildrone and NOAA-PMEL Case Study and Future
 1547 Considerations to Expand to Global Scale Observing. *Front. Mar. Sci.*, **6**, 448.
 1548 Mémin, E. 2014: Fluid flow dynamics under location uncertainty. *Geophysical & Astrophysical*
 1549 *Fluid Dynamics*, **108**, 119-146.
 1550 Menary, M. B., and Coauthors, 2018: Preindustrial control simulations with HadGEM3-GC3.1
 1551 for CMIP6. *J. Adv. Model. Earth Syst.*, **10**, 3049– 3075.
 1552 Messenger, C., and S. Swart, 2016: Significant atmospheric boundary layer change observed
 1553 above an Agulhas Current warm core eddy. *Adv. Meteor.*, 2016, 3659657.
 1554 Mey, R. D., N. D. Walker, and M. R. Jury, 1990: Surface heat fluxes and marine boundary layer
 1555 modification in the Agulhas Retroflexion Region. *J. Geophys. Res.*, **95**, 15 997–16 015.

- 1556 Minobe, S., A. Kuwano-Yoshida, N. Komori, S.-P. Xie, and R. J. Small, 2008: Influence of the
1557 Gulf Stream on the troposphere. *Nature*, **452**, 206–209.
- 1558 Minobe, S., M. Miyashita, A. Kuwano-Yoshida, H. Tokinaga, and S.-P. Xie, 2010: Atmospheric
1559 response to the Gulf Stream: Seasonal variations. *J. Climate*, **23**, 3699–3719.
- 1560 Moreno-Chamarro, E., L.-P. Caron, P. Ortega, S. Loosveldt Tomas, and M. J. Roberts, 2021:
1561 Can we trust CMIP5/6 future projections of European winter precipitation? *Environ. Res.*
1562 *Lett.*, **16**, 054063.
- 1563 Moreton, S., D. Ferreira, M. Roberts, and H. Hewitt, 2021: Air-Sea Turbulent Heat Flux
1564 Feedback over Mesoscale Eddies. *Geophys. Res. Lett.*, **48**, e2021GL095407.
- 1565 Nadiga, B. T., 2008: Orientation of eddy fluxes in geostrophic turbulence. *Phil. Trans. R. Soc.*
1566 *A.*, **366**, 2489–2508.
- 1567 Nakamura H., T. Sampe, Y. Tanimoto, and A. Shimpo, 2004: Observed associations among
1568 storm tracks, jet streams and midlatitude oceanic fronts. “Earth’s climate: the ocean-
1569 atmosphere interaction”. *AGU Geophys Monogr.*, **147**, 329–346.
- 1570 Nakamura, H., T. Sampe, A. Goto, W. Ohfuchi, and S.-P. Xie, 2008: On the importance of
1571 midlatitude oceanic frontal zones for the mean state and dominant variability in the
1572 tropospheric circulation. *Geophys. Res. Lett.*, **35**, L15709.
- 1573 Nakamura, H., and A. Shimpo, 2004: Seasonal Variations in the Southern Hemisphere Storm
1574 Tracks and Jet Streams as Revealed in a Reanalysis Dataset. *J. Climate*, **17**, 1828–1844.
- 1575 Nakamura, H., A. Nishina, and S. Minobe, 2012: Response of storm tracks to bimodal Kuroshio
1576 path states south of Japan. *J. Climate*, **25**, 7772–7779.
- 1577 Nakamura, H., and Coauthors, 2015: “Hot Spots” in the climate system—new developments in
1578 the extratropical ocean-atmosphere interaction research: a short review and an
1579 introduction. *J. Oceanogr.*, **71**, 463–467.
- 1580 Nakayama, M., H. Nakamura, and F. Ogawa, 2021: Impacts of a Midlatitude Oceanic Frontal
1581 Zone for the Baroclinic Annular Mode in the Southern Hemisphere. *J. Climate*, **34**, 7389-
1582 7408.
- 1583 Nkwinkwa Njouodo, A. S., S. Koseki, N. Keenlyside, and M. Rouault, 2018: Atmospheric
1584 signature of the Agulhas Current. *Geophys. Res. Lett.*, **45**, 5185–5193.
- 1585 Nonaka, M., H. Nakamura, B. Taguchi, N. Komori, A. Yoshida-
1586 Kuwano, and K. Takaya, 2009: Air-sea heat exchanges characteristic to a prominent

1587 midlatitude oceanic front in the South Indian Ocean as simulated in a high-resolution
1588 coupled GCM. *J. Climate*, **22**, 6515–6535.

1589 Omand, M. M., E. A. D’Asaro, C. M. Lee, M.-J. Perry, N. Briggs, I. Cetinić, and A. Mahadevan,
1590 2015: Eddy-driven subduction exports particulate organic carbon from the spring bloom.
1591 *Science*, **348**, 222-225.

1592 Olivier, L., and Coauthors, 2021: Impact of North Brazil Current rings on air-sea CO₂ flux
1593 variability in winter 2020. *Biogeosciences*, <https://doi.org/10.5194/bg-2021-269>.

1594 O’Neill, L. W., D. B. Chelton, and S. K. Esbensen, 2003: Observations of SST-induced
1595 perturbations of the wind stress field over the Southern Ocean on seasonal timescales. *J.*
1596 *Climate*, **16**, 2340– 2354.

1597 O’Neill, L. W., D. B. Chelton, and S. K. Esbensen, 2010: The effects of SST-induced wind speed
1598 and direction gradients on mid-latitude surface vorticity and divergence. *J. Climate*, **23**,
1599 255-281.

1600 O’Neill, L. W., D. B. Chelton, and S. K. Esbensen, 2012: Covariability of surface wind and
1601 stress responses to sea surface temperature fronts. *J. Climate*, **25**, 5916–5942.

1602 O’Neill, L. W., 2012: Wind Speed and Stability Effects on Coupling between Surface
1603 Wind Stress and SST Observed from Buoys and Satellites. *J. Climate*, **25**, 1544-1569.

1604 O’Neill, L. W., T. Haack, and T. Durland, 2015: Estimation of time-averaged surface divergence
1605 and vorticity from satellite ocean vector winds. *J. Climate*, **28**, 7596–7620.

1606 O’Neill, L. W., T. Haack, D. B. Chelton, and E. D. Skillingstad, 2017: The Gulf Stream
1607 Convergence Zone in the time-mean winds. *J. Atmos. Sci.*, **74**, 2383-2412.

1608 O’Reilly, C. H., and A. Czaja, 2015: The response of the Pacific storm track and atmospheric
1609 circulation to Kuroshio Extension variability. *Quart. J. Roy. Met. Soc.*, **141**, 52–66.

1610 O’Reilly, C. H., S. Minobe, and A. Kuwano-Yoshida, 2016: The influence of the Gulf Stream on
1611 wintertime European blocking. *Clim. Dyn.*, **47**, 1545–1567.

1612 O’Reilly, C. H., S. Minobe, A. Kuwano-Yoshida, and T. Woollings, 2017: The Gulf Stream
1613 influence on wintertime North Atlantic jet variability. *Quart. J. Roy. Meteor. Soc.*, **143**,
1614 173–183.

1615 Pacanowski, R. C., 1987: Effect of Equatorial Currents on Surface Stress. *J. Phys.*
1616 *Oceanogr.*, **17**, 833-838.

1617 Paduan, J. D., and L. Washburn, 2013: High-Frequency Radar Observations of Ocean Surface
1618 Currents. *Ann. Rev. Mar. Sci.*, **5**, 115-136.

1619 Palmer, T. N., and Z. Sun, 1985: A modeling and observational study of the relationship between
1620 sea-surface temperature in the northwest Atlantic and the atmospheric general circulation,
1621 *Quart. J. Roy. Meteor. Soc.*, **111**, 947-975.

1622 Parfitt, R., A. Czaja, S. Minobe, and A. Kuwano-Yoshida, 2016: The atmospheric frontal
1623 response to SST perturbations in the Gulf Stream region. *Geophys. Res. Lett.*, **43**, 2299–
1624 2306.

1625 Parfitt, R., and A. Czaja, 2016: On the contribution of synoptic transients to the mean
1626 atmospheric state in the Gulf Stream region. *Quart. J. Roy. Met. Soc.*, **142**, 1554–1561.

1627 Parfitt, R., and H. Seo, 2018: A New Framework for Near-Surface Wind Convergence over the
1628 Kuroshio Extension and Gulf Stream in Wintertime: The Role of Atmospheric
1629 Fronts. *Geophys. Res. Lett.*, **45**, 9909–9918.

1630 Peng, S., A. Robinson, and M. P. Hoerling, 1997: The modeled atmospheric response to
1631 midlatitude SST anomalies and its dependence on background circulation states. *J.*
1632 *Climate*, **10**, 971–987.

1633 Penny, S. G., and T. Hamill, 2017: Coupled data assimilation for integrated Earth system
1634 analysis and prediction. *Bull. Amer. Meteor. Soc.*, **97**, ES169–ES172.

1635 Perlin, N., S. P. de Szoeke, D. B. Chelton, R. M. Samelson, E. D. Skyllingstad, and L. W.
1636 O’Neill, 2014: Modeling the Atmospheric Boundary Layer Wind Response to Mesoscale
1637 Sea Surface Temperature Perturbations. *Mon. Wea. Rev.*, **142**, 4284–4307.

1638 Pezzi, L. P., R. B. Souza, M. S. Dourado, C. A. E. Garcia, M. M. Mata, and M. A. F. Silva-Dias,
1639 2005: Ocean-atmosphere in situ observations at the Brazil-Malvinas Confluence region.
1640 *Geophys. Res. Lett.*, **32**, L22603.

1641 Pezzi, L. P., and Coauthors, 2021: Oceanic eddy-induced modifications to air-sea heat and
1642 CO₂ fluxes in the Brazil-Malvinas Confluence. *Sci. Rep.*, **11**, 10648.

1643 Piazza, M., L. Terray, J. Boé, E. Maisonnave, and E. Sanchez- Gomez, 2016: Influence of small-
1644 scale North Atlantic sea surface temperature patterns on the marine boundary layer and
1645 free troposphere: A study using the atmospheric ARPEGE model. *Climate Dyn.*, **46**,
1646 1699–1717.

1647 Plagge, A. M., D. Vandemark, and B. Chapron, 2012: Examining the Impact of Surface Currents
1648 on Satellite Scatterometer and Altimeter Ocean Winds. *J. Atmos. Oceanic Tech.*, **29**,
1649 1776-1793.

1650 Polvani, L. M., D. W. Waugh, G. J. P. Correa, and S. Son, 2011: Stratospheric ozone depletion:
1651 The main driver of 20th century atmospheric circulation changes in the southern
1652 hemisphere, *J. Climate*, **24**, 795–812.

1653 Polverari, F., M. Portabella, W. Lin, J. W. Sapp, A. Stoffelen, Z. Jelenak, and P. S. Chang, 2021:
1654 On High and Extreme Wind Calibration Using ASCAT. *IEEE Trans. Geosci. Remote*
1655 *Sens.*, 0.1109/TGRS.2021.3079898

1656 Quinn, P. K., and Coauthors, 2021: Measurements from the RV Ronald H. Brown and
1657 related platforms as part of the Atlantic Tradewind Ocean-Atmosphere Mesoscale
1658 Interaction Campaign (ATOMIC). *Earth Syst. Sci. Data*, **13**, 1759–1790.

1659 Reason, C. J. C., 2001: Evidence for the influence of the Agulhas Current on regional
1660 atmospheric circulation patterns. *J. Climate*, **14**, 2769–2778.

1661 Reichl, B. G., and Deike, L., 2020: Contribution of sea-state dependent bubbles to air-sea carbon
1662 dioxide fluxes. *Geophys. Res. Lett.*, **47**, e2020GL087267.

1663 Reeder, M. J., T. Spengler, and C. Spensberger, 2021: The Effect of Sea Surface Temperature
1664 Fronts on Atmospheric Frontogenesis. *J. Atmos. Sci.*, **78**, 1753-1771.

1665 Renault, L., J. C. McWilliams, A. F. Shchepetkin, F. Lemarié, D. Chelton, S. Illig, and A. Hall,
1666 2016a: Modulation of wind work by oceanic current interaction with the atmosphere. *J.*
1667 *Phys. Oceanogr.*, **46**, 1685–1704.

1668 Renault, L., M. J. Molemaker, J. Gula, S. Masson, and J. C. McWilliams, 2016b: Control and
1669 stabilization of the Gulf Stream by oceanic current interaction with the atmosphere. *J.*
1670 *Phys. Oceanogr.*, **46**, 3439–3453.

1671 Renault, L., J. C. McWilliams, and P. Penven, 2017a: Modulation of the Agulhas Current
1672 retroflection and leakage by oceanic current interaction with the atmosphere in coupled
1673 simulations. *J. Phys. Oceanogr.*, **47**, 2077–2100.

1674 Renault, L., J. C. McWilliams, and S. Masson, 2017b: Satellite observations of imprint of
1675 oceanic current on wind stress by air-sea coupling. *Sci. Rep.*, **7**, 17747.

1676 Renault, L., J. C. McWilliams, and J. Gula, 2018: Dampening of submesoscale currents by air-
1677 sea stress coupling in the Californian upwelling system. *Sci. Rep.*, **8**, 13388.

1678 Renault, L., S. Masson, V. Oerder, S. Jullien, and F. Colas, 2019a: Disentangling the mesoscale
1679 ocean-atmosphere interactions. *J. Geophys. Res. Oceans*, **124**, 2164–2178.

1680 Renault, L., P. Marchesiello, S. Masson, and J. C. McWilliams, 2019b: Remarkable control of
1681 western boundary currents by eddy killing, a mechanical air-sea coupling process.
1682 *Geophys. Res. Lett.*, **46**, 2743–2751.

1683 Renault, L., S. Masson, T. Arsouze, G. Madec, and J. C. McWilliams, 2020: Recipes for how to
1684 force oceanic model dynamics. *J. Adv. Modeling Earth Syst.*, **12**, e2019MS001715.

1685 Renault L., S. Masson, V. Oerder, F. Colas, and J.C. McWilliams, Modulation of the Oceanic
1686 Mesoscale Activity by the Mesoscale Thermal FeedBack, *In preparation*.

1687 Roberts, M. J., Hewitt, H. T., Hyder, P., Ferreira, D., Josey, S. A., Mizielinski, M., and Shelly,
1688 A., 2016: Impact of ocean resolution on coupled air-sea fluxes and large-scale
1689 climate, *Geophys. Res. Lett.*, **43**, 10,430– 10,438.

1690 Robinson, W., P. Chang, E. Chassignet, and S. Speich, 2020: *Ocean Mesoscale Eddy*
1691 *Interactions with the Atmosphere* (No. 2020-05). (J. Zhu and M. Patterson, Eds.).
1692 Washington, DC: U.S. CLIVAR Project Office. [doi:10.5065/ebjm-5q77](https://doi.org/10.5065/ebjm-5q77).

1693 Robinson, W., S. Speich, and E. Chassignet, 2018: Exploring the interplay between ocean eddies
1694 and the atmosphere, *Eos*, **99**, <https://doi.org/10.1029/2018EO100609>.

1695 Romero, L., D. Hypolite, and J. C. McWilliams, 2020: Submesoscale current effects on surface
1696 waves. *Ocean Modell.*, **153**, 101662.

1697 Rousseau, V., E. Sanchez-Gomez, R. Msadek, and M. Moine, 2021: Mechanisms shaping wind
1698 convergence under extreme synoptic situations over the Gulf Stream region. *J. Climate*,
1699 **34**, 9481-9500.

1700 Saba, V. S., and Coauthors, 2016: Enhanced warming of the Northwest Atlantic Ocean under
1701 climate change. *J. Geophys. Res. Oceans*, **121**, 118-132.

1702 Samelson R., E. Skillingstad, D. Chelton, S. Esbensen, L. O'Neill, and N. Thum, 2006: On the
1703 coupling of wind stress and sea surface temperature. *J. Climate*, **19**, 1557-1566.

1704 Samelson, R. M., L. W. O'Neill, D. B. Chelton, E. D. Skillingstad, P. L. Barbour, and S. M.
1705 Durski, 2020: Surface Stress and Atmospheric Boundary Layer Response to Mesoscale
1706 SST Structure in Coupled Simulations of the Northern California Current System. *Mon.*
1707 *Wea. Rev.*, **148**, 259-287.

- 1708 Sampe, T., and S.-P. Xie, 2007: Mapping high sea winds from space: A global climatology. *Bull.*
1709 *Amer. Meteor. Soc.*, **88**, 1965-1978.
- 1710 Saviano, S., and Coauthors, 2021: Wind Direction Data from a Coastal HF Radar System in the
1711 Gulf of Naples (Central Mediterranean Sea, *Remote Sens.*, **13**, 1333.
- 1712 Schneider, N., and B. Qiu, 2015: The atmospheric response to weak sea surface temperature
1713 fronts. *J. Atmos. Sci.*, **72**, 3356–3377.
- 1714 Schneider, N., 2020: Scale and Rossby Number Dependence of Observed Wind Responses to
1715 Ocean-Mesoscale Sea Surface Temperatures. *J. Climate*, **77**, 3171-3192.
- 1716 Scott, R. B., and Y. Xu, 2009: An update on the wind power input to the surface geostrophic
1717 flow of the World Ocean. *Deep-Sea Res.*, **56**, 295–304.
- 1718 Seager, R., Y. Kushnir, N. H. Naik, M. A. Cane, and J. Miller, 2001: Wind-Driven Shifts in the
1719 Latitude of the Kuroshio–Oyashio Extension and Generation of SST Anomalies
1720 on Decadal Timescales. *J. Climate*, **14**, 4249-4265.
- 1721 Seager, R., and I. R. Simpson, 2016: Western boundary currents and climate change. *J. Geophys.*
1722 *Res. Oceans*, **121**, 7212–7214.
- 1723 Seo, H., M. Jochum, R. Murtugudde, A. J. Miller, and J. O. Roads, 2007: Feedback of Tropical
1724 Instability Wave - induced Atmospheric Variability onto the Ocean. *J. Climate*, **20**, 5842-
1725 5855.
- 1726 Seo, H., Y.-O. Kwon, and J.-J. Park, 2014: On the effect of the East/Japan Sea SST variability on
1727 the North Pacific atmospheric circulation in a regional climate model. *J. Geophys. Res.*
1728 *Atmos.*, **119**, 418–444.
- 1729 Seo, H., A. J. Miller, and J. R. Norris, 2016: Eddy-wind interaction in the California Current
1730 System: dynamics and impacts. *J. Phys. Oceanogr.*, **46**, 439-459.
- 1731 Seo, H., 2017: Distinct influence of air-sea interactions mediated by mesoscale sea surface
1732 temperature and surface current in the Arabian Sea. *J. Climate*, **30**, 8061-8079.
- 1733 Seo, H., Y.-O. Kwon, T. M. Joyce, and C. C. Ummenhofer, 2017: On the predominant nonlinear
1734 response of the extratropical atmosphere to meridional shift of the Gulf Stream. *J.*
1735 *Climate*, **30**, 9679-9702.
- 1736 Seo, H., A. C. Subramanian, H. Song, and J. S. Chowdary, 2019: Coupled effects of ocean
1737 current on wind stress in the Bay of Bengal: Eddy energetics and upper ocean
1738 stratification. *Deep-Sea Res. II*, **168**, 104617.

1739 Seo, H., H. Song, L. W. O'Neill, M. R. Mazloff, and B. D. Cornuelle, 2021: Impacts of ocean
1740 currents on the South Indian Ocean extratropical storm track through the relative wind
1741 effect. *J. Climate*, **34**, 9093-9113.

1742 Sheldon, L., A. Czaja, B. Vanni re, C. Morcrette, B. Sohet, M. Casado, and D. Smith, 2017: A
1743 warm path to Gulf Stream–troposphere interactions. *Tellus*, **69**, 1–13.

1744 Shi, Q., and M. A. Bourassa, 2019: Coupling Ocean Currents and Waves with Wind Stress over
1745 the Gulf Stream. *Remote Sens.*, **11**, 1476.

1746 Shinoda, T., S. Pei, W. Wang, J. X. Fu. R.-C. Lien, H. Seo, and A. Soloviev, 2021: Climate
1747 Process Team: improvement of ocean component of NOAA Climate Forecast System
1748 relevant to Madden-Julian Oscillation simulations. *J. Adv. Model. Earth Syst.*, **13**,
1749 e2021MS002658.

1750 Shroyer, E., and Coauthors, 2021: Bay of Bengal Intraseasonal Oscillation and the 2018
1751 Monsoon Onset. *Bull. Amer. Meteor. Soc.*, **102**, E1936-E1951.

1752 Singleton, A. T., and C. J. C. Reason, 2006: Numerical simulations of a severe rainfall event
1753 over the Eastern Cape coast of South Africa: Sensitivity to sea surface temperature and
1754 topography. *Tellus*, **58A**, 335–367.

1755 Siqueira, L., and B. P. Kirtman, 2016: Atlantic near-term climate variability and the role of a
1756 resolved Gulf Stream. *Geophys. Res. Lett.*, **43**, 3964–3972.

1757 Siqueira, L., B. P. Kirtman, and L. C. Laurindo, 2021: Forecasting Remote Atmospheric
1758 Responses to Decadal Kuroshio Stability Transitions. *J. Climate*, **34**, 379–395.

1759 Skillingstad, E. D., D. Vickers, L. Mahrt, and R. Samelson, 2007: Effects of mesoscale sea-
1760 surface temperature fronts on the marine atmospheric boundary layer. *Boundary-Layer
1761 Meteorol.*, **123**, 219–237.

1762 Skillingstad, E. D., and J. B. Edson, 2009: Large-eddy simulation of moist convection during a
1763 cold-air outbreak over the Gulf Stream. *J. Atmos. Sci.*, **66**(5), 1274-1293.

1764 Skillingstad, E. D., S. P. de Szoeke, and L. W. O'Neill, 2019: Modeling the Transient Response
1765 of Tropical Convection to Mesoscale SST Variations. *J. Atmos. Sci.*, **76**, 1227-1244.

1766 Small, R. J., S.-P. Xie, Y. Wang, S. K. Esbensen, and D. Vickers, 2005a: Numerical Simulation
1767 of Boundary Layer Structure and Cross-Equatorial Flow in the Eastern Pacific. *J. Atmos.
1768 Sci.*, **62**(6), 1812-1830.

1769 Small, R. J., S.-P. Xie, and J. Hafner, 2005b: Satellite observations of mesoscale ocean features
1770 and copropagating atmospheric surface fields in the tropical belt. *J. Geophys. Res.*, **110**,
1771 C02021.

1772 Small, R. J., S. de Szoeke, S.-P. Xie, L. O'Neill, H. Seo, Q. Song, P. Cornillon, M. Spall, and S.
1773 Minobe, 2008: Air-Sea Interaction over Ocean Fronts and Eddies. *Dyn. Atmos. Oceans*,
1774 **45**, 274-319.

1775 Small, R. J., R. Msadek, Y. Kwon, J. F. Booth, and C. Zarzycki, 2019: Atmosphere surface
1776 storm track response to resolved ocean mesoscale in two sets of global climate model
1777 experiments. *Clim. Dyn.*, **52**, 2067–2089.

1778 Smirnov, D., M. Newman, M. A. Alexander, Y.-O. Kwon, and C. Frankignoul, 2015:
1779 Investigating the local atmospheric response to a realistic shift in the Oyashio sea surface
1780 temperature front. *J. Climate*, **28**, 1126–1147.

1781 Song, H., J. Marshall, P. Gaube, and D. J. McGillicuddy, 2015: Anomalous chlorofluorocarbon
1782 uptake by mesoscale eddies in the Drake Passage region. *J. Geophys. Res. Oceans*, **120**,
1783 1065-1078.

1784 Song, H., J. Marshall, M. J. Follows, S. Dutkiewicz and G. Forget, 2016: Source waters for the
1785 highly productive Patagonian shelf in the southwestern Atlantic. *J. Mar. Syst.*, **158**, 120-
1786 128.

1787 Song, Q., P. Cornillon, and T. Hara, 2006: Surface wind response to oceanic fronts. *J. Geophys.*
1788 *Res.*, **111**, C12006.

1789 Song, Q., D. B. Chelton, S. K. Esbensen, N. Thum, and L. W. O'Neill, 2009: Coupling between
1790 Sea Surface Temperature and Low-Level Winds in Mesoscale Numerical Models. *J.*
1791 *Climate*, **22**, 146-164.

1792 Song, Q., D. B. Chelton, S. K. Esbensen, and A. R. Brown, 2017: An Investigation of the
1793 Stability Dependence of SST-Induced Vertical Mixing over the Ocean in the Operational
1794 Met Office Model. *J. Climate*, **30**, 91-107.

1795 Song, H., J. Marshall, D. J. McGillicuddy Jr., and H. Seo, 2020: The impact of the current-wind
1796 interaction on the vertical processes in the Southern Ocean. *J. Geophys. Res.-*
1797 *Oceans*, **125**, e2020JC016046.

1798 Souza, R., L. Pezzi, S. Swart, F. Oliveira, and M. Santini, 2021: Air-Sea Interactions over Eddies
1799 in the Brazil-Malvinas Confluence. *Remote Sens.*, **13**, 1335.

1800 Spall, M. A., 2007: Effect of sea surface temperature-wind stress coupling on baroclinic
1801 instability in the ocean. *J. Phys. Oceanogr.*, **37**, 1092-1097.

1802 Sprintall, J., V. J. Coles, K. A. Reed, A. H. Butler, G. R. Foltz, S. G. Penny, and H. Seo, 2020:
1803 Best practice strategies for process studies designed to improve climate modeling. *Bull.*
1804 *Amer. Meteor. Soc.*, **101**, E1842–1850.

1805 Stevens, B., and Coauthors, 2003: Dynamics and Chemistry of Marine Stratocumulus –
1806 DYCOMS-II. *Bull. Amer. Meteor. Soc.*, **84**, 579–594.

1807 Stevens, B., and Coauthors, 2019: DYAMOND: the DYnamics of the Atmospheric general
1808 circulation modeled on non-hydrostatic domains. *Prog. Earth Planet Sci.*, **6**, 61.

1809 Stevens, B., and Coauthors, 2021: EUREC4A. *Earth System Science Data*, **13**, 4067-4119.

1810 Stoffelen, A., R. Kumar, J. Zou, V. Karaev, P. S. Chang, and E. Rodriguez, 2019: Ocean Surface
1811 Vector Wind Observations. In: Barale V., Gade M. (eds) Remote Sensing of the Asian
1812 Seas. Springer, Cham. https://doi.org/10.1007/978-3-319-94067-0_24.

1813 Su, Z., and Coauthors, 2018: Ocean submesoscales as a key component of the global heat
1814 budget. *Nat. Commun.*, **9**, 775.

1815 Sugimoto, S., B. Qiu, and N. Schneider, 2021: Local Atmospheric Response to the Kuroshio
1816 Large Meander Path in Summer and Its Remote Influence on the Climate of Japan. *J.*
1817 *Climate*, **34**, 3571-3589.

1818 Sullivan, P., and J. C. McWilliams, 2019: Langmuir turbulence and filament frontogenesis in the
1819 oceanic surface boundary layer. *J. Fluid Mech.*, **879**, 512-553.

1820 Sullivan, P. P., J. C. McWilliams, J. C. Weil, E. G. Patton, and H. J. S. Fernando, 2020: Marine
1821 Boundary Layers above Heterogeneous SST: Across-Front Winds. *J. Atmos. Sci.*, **77**,
1822 4251-4275.

1823 Sullivan, P. P., J. C. McWilliams, J. C. Weil, E. G. Patton, and H. J. S. Fernando, 2021: Marine
1824 Boundary Layers above Heterogeneous SST: Alongfront Winds. *J. Atmos. Sci.*, **78**, 3297-
1825 3315.

1826 Sun, X., and R. Wu, 2021: Spatial scale dependence of the relationship between turbulent surface
1827 heat flux and SST. *Clim. Dyn.*, <https://doi.org/10.1007/s00382-021-05957-9>.

1828 Suzuki, N., B. Fox-Kemper, P. E. Hamlington, and L. P. Van Roekel, 2016: Surface waves affect
1829 frontogenesis. *J. Geophys. Res. Oceans*, **121**, 1-28.

1830 Sweet, W., R. Fett, J. Kerling, and P. La Violette, 1981: Air-sea interaction effects in the lower
1831 troposphere across the north wall of the Gulf Stream. *Mon. Wea. Rev.*, **109**, 1042–1052.

1832 Taguchi, B., S.-P. Xie, N. Schneider, M. Nonaka, H. Sasaki, and Y. Sasai, 2007: Decadal
1833 variability of the Kuroshio Extension: Observations and an eddy-resolving model
1834 hindcast. *J. Climate*, **20**, 2357–2377.

1835 Taguchi, B., H. Nakamura, M. Nonaka, K. Komori, A. Kuwano-Yoshida, K. Takaya, and A.
1836 Goto, 2012: Seasonal evolutions of atmospheric response to decadal SST anomalies in
1837 the North Pacific subarctic frontal zone: observations and a coupled model simulation. *J.*
1838 *Climate*, **25**, 111–139.

1839 Takatama, K., S. Minobe, M. Inatsu, and R. J. Small, 2012: Diagnostics for near-surface wind
1840 convergence/divergence response to the Gulf Stream in a regional atmospheric model.
1841 *Atmos. Sci. Lett.*, **13**, 16–21.

1842 Takatama, K., S. Minobe, M. Inatsu, and R. J. Small, 2015: Diagnostics for near-surface wind
1843 response to the Gulf Stream in a regional atmospheric model. *J. Climate*, **28**, 238–255.

1844 Takatama, K., and N. Schneider, 2017: The Role of Back Pressure in the Atmospheric Response
1845 to Surface Stress Induced by the Kuroshio. *J. Atmos. Sci.*, **74**, 597–615.

1846 Thomson, J., 2012: Wave Breaking Dissipation Observed with “SWIFT” Drifters. *J. Atmos.*
1847 *Oceanic Technol.*, **29**, 1866–1882.

1848 Thomson, J., and J. Girton, 2017: Sustained measurements of Southern Ocean air-sea coupling
1849 from a Wave Glider autonomous surface vehicle. *Oceanogr.*, **30**, 104–109.

1850 Thum, N., S. K. Esbensen, D. B. Chelton, and M. J. McPhaden, 2002: Air-sea heat exchange
1851 along the northern sea surface temperature front in the eastern tropical Pacific. *J.*
1852 *Climate*, **15**, 3361–3378.

1853 Tokinaga, H., Y. Tanimoto, and S.-P. Xie, 2005: SST-Induced Surface Wind Variations over the
1854 Brazil–Malvinas Confluence: Satellite and In Situ Observations. *J. Climate*, **18**, 3470–
1855 3482.

1856 Trenberth, K. E., and D. J. Shea, 2005: Relationships between precipitation and surface
1857 temperature. *Geophys. Res. Lett.*, **32**, L14703.

1858 Tokinaga, H., Y. Tanimoto, S.-P. Xie, T. Sampe, H. Tomita, and H. Ichikawa, 2009: Ocean
1859 Frontal Effects on the Vertical Development of Clouds over the Western North Pacific:
1860 In Situ and Satellite Observations. *J. Climate*, **22**, 4241–4260.

- 1861 Trindade, A., M. Portabella, A. Stoffelen, W. Lin, and A. Verhoef, 2020: ERAstar: A High-
1862 Resolution Ocean Forcing Product. *IEEE Transactions on Geoscience and Remote*
1863 *Sensing*, **58**, 1337–1347.
- 1864 Trowbridge, J., R. Weller, D. Kelley, E. Dever, A. Plueddemann, J. A. Barth, and O. Kawka,
1865 2019: The Ocean Observatories Initiative. *Front. Mar. Sci.*, **6**, 74.
- 1866 Tsopouridis, L., C. Spensberger, and T. Spengler, 2021: Cyclone intensification in the Kuroshio
1867 region and its relation to the sea surface temperature front and upper-level forcing. *Quart.*
1868 *J. Roy. Met. Soc.*, **147**, 485-500.
- 1869 Vannière, B., A. C. H. Dacre, and T. Woollings, 2017: A “cold path” for the Gulf Stream–
1870 troposphere connection. *J. Climate*, **30**, 1363–1379.
- 1871 Vecchi, G. A., S.-P. Xie, and A. S. Fischer, 2004: Ocean-atmosphere covariability in the western
1872 Arabian Sea. *J. Climate*, **17**, 1213-1224.
- 1873 Verdy, A., and M. R. Mazloff, 2017: A data assimilating model for estimating Southern Ocean
1874 biogeochemistry. *J. Geophys. Res. Oceans*, **122**, 6968– 6988.
- 1875 Villas Bôas, A. B., O. T. Sato, A. Chaigneau, and G. P. Castelão, 2015: The signature of
1876 mesoscale eddies on the air-sea turbulent heat fluxes in the South Atlantic Ocean.
1877 *Geophys. Res. Lett.*, **42**, 1856–1862.
- 1878 Villas Bôas, A. B., and Coauthors, 2019: Integrated Observations of Global Surface Winds,
1879 Currents, and Waves: Requirements and Challenges for the Next Decade. *Front. Mar.*
1880 *Sci.*, **6**, 425.
- 1881 Villas Bôas, A. B., and W. Young, 2020: Directional diffusion of surface gravity wave action by
1882 ocean macroturbulence. *J. Fluid Mech.*, **890**, R3.
- 1883 Villas Bôas, A. B., B. D. Cornuelle, M. R. Mazloff, S. T. Gille, and F. Ardhuin, 2020: Wave–
1884 Current Interactions at Meso- and Submesoscales: Insights from Idealized Numerical
1885 Simulations. *J. Phys. Oceanogr.*, **50**, 3483-3500.
- 1886 Villas Bôas, A. B., and N. Pizzo, 2021: The geometry, kinematics, and dynamics of the two-way
1887 coupling between wind, waves, and currents. *US CLIVAR Variations*, **19**, 18-26.
- 1888 Wai, M. M., and S. A. Stage, 1989: Dynamical analyses of marine atmospheric boundary layer
1889 structure near the Gulf Stream oceanic front. *Quart. J. Roy. Met. Soc.*, **115**, 29–44.

1890 Wallace, J. M., T. P. Mitchell, and C. Deser, 1989: The influence of sea surface temperature on
1891 sea surface wind in the eastern equatorial Pacific. Seasonal and interannual variability. *J.*
1892 *Climate*, **2**, 1492–1499.

1893 Wang, Y., C. Wang, H. Zhang, Y. Dong, and S. Wei, 2019: SAR Dataset of Ship Detection for
1894 Deep Learning under Complex Backgrounds. *Remote Sens.*, **11**, 765.

1895 Wang, Q., J. A. Kalogiros, S. R. Ramp, J. D. Paduan, G. Buzorius, and H. Jonsson, 2011: Wind
1896 Stress Curl and Coastal Upwelling in the Area of Monterey Bay Observed during AOSN-
1897 II. *J. Phys. Oceanogr.*, **41**, 857–877.

1898 Wang, Q., and Coauthors, 2018: CASPER: Coupled Air-Sea Processes and Electromagnetic
1899 (EM) ducting Research. *Bull. Amer. Meteor. Soc.*, **99**, 1449–1471.

1900 Wanninkhof, R., 1992: Relationship between wind speed and gas exchange over the ocean. *J.*
1901 *Geophys. Res.*, **97**, 7373–7382.

1902 Wanninkhof, R., W. E. Asher, D. T. Ho, C. Sweeney, and W. R. McGillis, 2009: Advances in
1903 quantifying air-sea gas exchange and environmental forcing. *Ann. Rev. Mar. Sci.*, **1**, 213–
1904 44.

1905 Wanninkhof, R., G. Park, D. B. Chelton, and C. M. Risien, 2011: Impact of Small-Scale
1906 Variability on Air-Sea CO₂ Fluxes. In *Gas Transfer at Water Surfaces*, 2010, edited by S.
1907 Komori, W. McGillis, and R. Kurose, 431–44. Kyoto University Press, Kyoto.

1908 Warner, T. T., M. N. Lakhtakia, J. D. Doyle, and R. A. Pearson, 1990: Marine atmospheric
1909 boundary layer circulations forced by Gulf Stream sea surface temperature gradients.
1910 *Mon. Wea. Rev.*, **118**, 309–323.

1911 Weaver, A. J., Coauthors, 2012: Stability of the Atlantic meridional overturning circulation: A
1912 model intercomparison. *Geophys. Res. Lett.*, **39**, L20709.

1913 Wenegrat, J. O., and R. S. Arthur, 2018: Response of the atmospheric boundary layer to
1914 submesoscale sea surface temperature fronts. *Geophys. Res. Lett.*, **45**, 13,505– 13,512.

1915 Wengel, C., and Coauthors, 2021: Future high-resolution El Niño/Southern Oscillation
1916 dynamics. *Nat. Clim. Chang.* **11**, 758–765.

1917 Willison, J., W. A. Robinson, and G. M. Lackmann, 2013: The Importance of Resolving
1918 Mesoscale Latent Heating in the North Atlantic Storm Track. *J. Atmos. Sci.*, **70**, 2234-
1919 2250.

1920 Wills, S. M., D. W. J. Thompson, and L. M. Ciasto, 2016: On the Observed Relationships
1921 between Variability in Gulf Stream Sea Surface Temperatures and the Atmospheric
1922 Circulation over the North Atlantic. *J. Climate*, **29**, 3719-3730.

1923 Wills, S. M., and D. W. J. Thompson, 2018: On the Observed Relationships between Wintertime
1924 Variability in Kuroshio–Oyashio Extension Sea Surface Temperatures and the
1925 Atmospheric Circulation over the North Pacific. *J. Climate*, **31**, 4669-468.

1926 Wineteer, A., H. S. Torres, and E. Rodriguez, 2020: On the surface current measurement
1927 capabilities of spaceborne Doppler scatterometry. *Geophys. Res. Lett.*, **47**,
1928 e2020GL090116.

1929 Winton, M., S. M. Griffies, B. L. Samuels, J. L. Sarmiento, and T. L. Frölicher, 2013:
1930 Connecting Changing Ocean Circulation with Changing Climate. *J. Climate*, **26**, 2268-
1931 2278.

1932 Woolf, D. K., 1993: Bubbles and the air-sea transfer velocity of gases. *Atmosphere-Ocean*, **31**,
1933 517–540.

1934 Woollings, T., J. M. Gregory, J. G. Pinto, M. Reyers, and D. J. Brayshaw, 2012: Response of the
1935 North Atlantic storm track to climate change shaped by ocean-atmosphere coupling. *Nat.*
1936 *Geosci.*, **5**, 313–317.

1937 Wu., R., B. P. Kirtman, and K. Pegion, 2006: Local Air-Sea Relationship in Observations and
1938 Model Simulations. *J. Climate*, **19**, 4914-4932.

1939 Xie, S.-P. 2004: Satellite observations of cool ocean-atmosphere interaction. *Bull. Amer. Meteor.*
1940 *Soc.*, **85**, 195–209.

1941 Xie, T., W. Perrie, and W. Chen, 2010: Gulf Stream thermal fronts detected by synthetic aperture
1942 radar. *Geophys. Res. Lett.*, **37**, L06601.

1943 Yang, H., G. Lohmann, W. Wei, M. Dima, M. Ionita, and J. Liu, 2016: Intensification and
1944 poleward shift of subtropical western boundary currents in a warming climate. *J.*
1945 *Geophys. Res. Oceans*, **121**, 4928–4945.

1946 Yu, L., 2019: Global air-sea fluxes of heat, fresh water, and momentum: energy budget closure
1947 and unanswered questions. *Ann. Rev. Mar. Sci.*, **11**, 227-248.

1948 Zanna, L., P. G. Porta Mana, J. Anstey, T. David, and T. Bolton, 2017: Scale-Aware
1949 Deterministic and Stochastic Parametrizations of Eddy-Mean Flow Interaction. *Ocean*
1950 *Modell.*, **111**, 66-80.